

**Method for Continuous Inspection of Product
Weight During Lyophilization**

by

Ellen Bridget O’Connell

Submitted to the Department of Mechanical Engineering
in partial fulfillment of the requirements for the degree of

Master of Science in Mechanical Engineering

at the

MASSACHUSETTS INSTITUTE OF TECHNOLOGY

September 2021

© Massachusetts Institute of Technology 2021. All rights reserved.

Signature of Author: _____
Department of Mechanical Engineering
August 6, 2021

Certified by: _____
Alexander H. Slocum
Walter M. May and A. Hazel May Professor of Mechanical Engineering
Thesis Supervisor

Accepted by: _____
Nicolas Hadjiconstantinou
Professor of Mechanical Engineering, Graduate Officer

Method for Continuous Inspection of Product Weight During Lyophilization

by

Ellen Bridget O'Connell

Submitted to the Department of Mechanical Engineering
on September 22, 2021 in partial fulfillment of the
requirements for the degree of

Master of Science in Mechanical Engineering

Abstract

During lyophilization, a freeze-drying process used to stabilize pharmaceuticals, vials filled with product go through stages to sublimate out the water contained in the initially frozen product. The final product is a solid with a low water content which is more stable for shipping. This work focused on a method for continuous inspection of product weight in vitro, specifically in the lyophilization context. Traditional batch lyophilizers cannot obtain continuous product weight data as a function of time during the lyophilization process on a vial specific basis (Laurens De Meyer, 2019). The weight-sensing approach developed presents an option for continuous or periodic interval collection of product weight data for the product in each vial. This method for continuous inspection of weight change of a product on a per vial basis allows for a much better understanding of the weight change over time and also opens up the possibility of altering process conditions to obtain a desired weight change over time profile for all vials.

In the larger lyophilization system for which this weight-measuring subsystem was designed the final product was required to be evaluated down to a 0.1% water content. There were additional system considerations such as viewing deflections, which could be related to weight changes, from the top of the system and strict limits on materials due to a need for sterility in the larger system. Largely as a result of these requirements a Keyence Laser Displacement Sensor was selected as the primary sensing method for deflection with an imaging/moiré approach as a secondary sensing method.

This thesis is focused on the options explored to measure product weight change through deflection of elastic structures used to support the vials during lyophilization. Ultimately, a Bent Spring wire approach was selected but this concept was heavily informed and inspired by Triangle Flexure and Diaphragm designs which were also explored but ultimately did not perform sufficiently given our strict deflection change requirement of at least 1mm. This 1mm deflection

change threshold allows us to evaluate the final product down to a 0.1% water content. The performance of the deflection approaches and designs were experimentally tested by incrementally altering the weight supported by the designs. The experimental results were also compared with calculated results and simulation results. The Bent Spring design met the deflection change requirement as well as the other functional requirements and design parameters for the larger system. The Bent Spring approach is a method for measuring weight change of product continuously in each vial while also being simple to prototype and manufacture.

Thesis Supervisor: Alexander H. Slocum

Title: Walter M. May and A. Hazel May Professor of Mechanical Engineering

Acknowledgements

I would like to thank my advisor Professor Alexander Slocum for his guidance and help throughout this work. As approaches and designs were rapidly evolving Professor Slocum provided invaluable advice and direction.

I would like to thank the entire team working on the lyophilization project for their help through this project and for always stepping up with recommendations and aid as needed.

Additionally, I would also like to thank the members of the Precision Engineering Research Group (PERG) who were very supportive and always open to design reviews and brainstorming sessions.

Lastly, I would like to thank my family and friends who have supported me. Thank you to my friends for working through tough psets and classes together. Thank you to my family for your encouragement and support.

Table of Contents

Abstract

Acknowledgements

Table of Contents

List of Figures

List of Tables

1. Introduction	11
Motivation	11
Background	11
1.1.1 General Design Requirements	11
1.1.2 Existing Sensor Review	15
2. Weight-sensing Deflection Subsystem Design, Fabrication, and Evaluation	15
Vial Spacing General Design Geometry	15
Retaining Posts	16
Bent Spring	17
2.1.1 Final Bent Spring Design	18
2.1.2 Prototyped and Tested Bent Spring Design	21
Triangle Flexure	38
2.1.3 Design and Tulip Array	40
Alternative Flexure	51
2.1.4 Design	51
Diaphragm	53
2.1.5 Design	54
2.1.6 Prototyping and Evaluation	65
3. Sensing	68
3.1.1 Laser Displacement Sensor	68
3.1.2 Imaging Displacement	69
4. Conclusion	72
5. Future Steps	72
6. Bibliography	73

List of Figures

Figure 1: Retaining Posts.	16
Figure 2: Bent Spring Layout.	18
Figure 3: Vial Holder Wire Connection.	19
Figure 4: Wire Mounts.	19
Figure 5: Wire Profile.	20
Figure 7: Bent Wire Experimental Setup.	22
Figure 8: Bent Spring, Spring Back Stainless Steel Experimental Results	23
Figure 9: Bent Spring Design Experimental Results with Multiple Runs.	24
Figure 10: Straight Spring Design with Low Mounting.	25
Figure 11: Straight Spring Design with Low Mounting Experimental Setup.	26
Figure 12: Straight Spring with Low Mounting Experimental Results.	26
Figure 13: Straight Spring with Low Mounting Prong Length.	27
Figure 14: Straight Spring with High Mounting Experimental Setup.	29
Figure 15: Straight Spring with High Mounting and Fixed Ends.	30
Figure 16: Straight Spring with High Mounting and Right-Angle Hard Stops Experimental Setup.	31
Figure 17: Straight Spring with High Mounting and Right-Angle Hard Stops Experimental Results.	32
Figure 18: Full and Partial Loop Designs and Prototypes.	33
Figure 19: Wire Bending Template.	34
Figure 20: Full Loop Simulation and Experimental Results.	36
Figure 21: Partial Loop Simulation and Experimental Results.	37
Figure 22: Full Loop Prototypes.	38
Figure 23: Tulip and Flat Flexure Designs.	39
Figure 24: Tulip Flexure Design.	40
Figure 25: Tulip Flexure Radiation Concentrator.	41
Figure 26: Tulip Flexure Stationary Sides.	42
Figure 27: Flat Base Flexure Design.	43
Figure 28: Flat Base Vial Array.	44
Figure 29: Tulip Base Vial Array.	44

Figure 30: Comparison Between Flat Base and Tulip Base Sublimation.....	45
Figure 31: Flat Base and Tulip Base Thermal Images.	46
Figure 32: Modular Designs for the Tulip and Flat Flexure Designs.	47
Figure 33: Tulip Petal Flexure Design.	48
Figure 34: Ideal Flat Integrated Flexure Design.....	49
Figure 35: Prototyped Flat Flexure Experiments.	50
Figure 36: Alternative Flexure Patterns.	51
Figure 38: Modified Corrugated Diaphragm Design.	61
Figure 39: Hexagonal Diaphragm Design.....	61
Figure 40: The Final Prototype 3D Printed Diaphragm Design.....	64
Figure 41: Pre-Curved Diaphragm Design.....	65
Figure 42: Pre-Curved Diaphragm Connection to Vial Holder.	65
Figure 44: BMF Prototypes.....	66
Figure 45: Image of Cross-Section of BMF Diaphragm.....	67
Figure 46: 3D Printed Diaphragm Experimental Results.....	67
Figure 47: Keyence Laser Displacement Sensor Spot.	69
Figure 49: Displacement of Springs From Above.....	70
Figure 50: Example of Measuring Relative Areas for Wire Displacement.	71
Figure 51: Example of Partial Loop Displacement.....	71

List of Tables

Table 1: Process Metrics.	14
Table 2: Straight Spring with Low Mounting Prong Length and Diameter Table.	28
Table 3: Summary of Full and Partial Loop Simulations.	35
Table 4: Tulip vs. Flat Experimental Conditions.	45
Table 5: Alternative Flexure Patterns and Simulated Deflection Changes.	53
Table 6: Diaphragm Images and Simulations.	56
Table 7: Diaphragm Simulation Results.	57
Table 8: Potential Injection Molding Materials.	58
Table 9: Diaphragm Simulations with Injection Molding Materials.	59
Table 10: HDPE Diaphragm Simulation Results.	60
Table 11: BMF 3D Printed Diaphragm Simulation Results.	62
Table 12: 3D Printed Diaphragm Geometries.	63
Table 13: 3D Printed Diaphragm Design Simulation Results - Material Thickness.	64

1. Introduction

Motivation

In traditional lyophilizers a batch process is used in which the vial-specific product weight, and therefore the specific conditions a vial's product experienced, is unknown during the lyophilization process. Batch lyophilizers often have variability between product in vials (Laurens De Meyer, 2019). Recently, there has been work done to develop continuous lyophilization systems and it has been seen that more uniform product is created with such an approach (Luigi, 2019). With the development of continuous lyophilization systems and the desire for more uniform product vial-to-vial and more intravial product uniformity there is an opportunity for a vial specific weight-sensing approach to provide continuous product weight data. This continuous product weight data can be used to understand the lyophilization process progress in each vial which can in turn inform adjustments to the system controls to ensure that the product is uniform within a specific vial and across an array of vials.

The larger lyophilization system for which this continuous weight-sensing approach was designed had strict requirements related to the characteristics of the larger system. Key among these requirements, described in greater detail below, was the ability to sense the weight change from looking above the vials without disrupting the lyophilization process. Traditionally, the weight of a product would be measured by a scale below the vial but due to the structure of the larger lyophilization system having a scale under the vials was not possible which necessitated looking at another option for reading weight change. Deflection was selected as a change that would happen with product weight changes and could be measured from above. Because this weight-sensing subsystem was to integrate into the larger lyophilization system there were strict material, particulate, and sterility requirements.

Background

1.1.1 General Design Requirements

The major design requirements for the weight-sensing deflection subsystem came from requirements which applied to the entirety of the lyophilization system and requirements which were specific to the weight-sensing approach.

1.1.1.1 Material Requirements

The weight-sensing subsystem is part of a lyophilization system. As such, sterility and compatibility with biologics were critical. Steam cleaning is often the method for sterilizing pharmaceutical systems between runs with differing biologics and the steam cleaning sterilization process set the upper bound for the temperature requirement for the material selection. The lower bound for the temperature requirement came from a step in the larger system where temperatures as low as -40 degC may be briefly experienced. The temperature requirement and the compatibility with biologics requirement which come directly from the lyophilization system meant that all materials used in the weight-sensing subsystem needed to be able to withstand the range of temperatures and withstand cycling between the two temperature extremes over runs of the larger system. Additionally, thermal expansion characteristics were an important consideration.

Another major material requirement consideration was a result of stages in the lyophilization system in which the weight-sensing subsystem would be under vacuum (down to approximately 1 Pa). Each material in the weight-sensing subsystem needed to be stable in a vacuum and not release any toxic or potential contaminants through off gassing.

A very common material in pharmaceutical systems is stainless steel and the larger system has strong magnets which meant that a strict material requirement was for the material to not be magnetic. As described above, the lower bound on the temperature experienced by the weight-sensing subsystem was assumed to be -40 degC. Even non-magnetic forms of stainless steel can become magnetic when exposed to low temperatures. It was critical that the materials selected for the weight-sensing subsystem would not become magnetic as a result of the cold temperatures. If the stainless steel did become magnetic it would no longer function correctly when exposed to the strong magnets of the larger system. Typically, stainless steels such as 316L need to reach cryogenic temperatures to go through a martensitic transformation and become magnetic (Cedric Garion, 2006). It was not expected that the stainless steel in this system should experience temperatures low enough to cause a martensitic transformation, but it was a consideration as the required temperature for this transformation varies depending on material.

1.1.1.2 Continuous Vial Specific Reading Requirements

A significant requirement of the weight-sensing subsystem is that weight readings should not disrupt the overall process and each vial's individual product weight change should be

observable. The ability to continuously obtain weight measurements for each vial allows for evaluation of the progress the vials and product are experiencing. Traditionally this data is not available either continuously or on a per vial basis. Because the vials and their contents are going through various stages and conditions in the larger system viewing deflection changes, which can be related to weight changes, from above the vials was a requirement.

1.1.1.3 Deflection Requirements

Because the weight-sensing subsystem was based on changes in deflection as water is removed from the product but the weight of the system is dominated by the vial holding the product, the required deflection was a key design requirement. The final product, the vial's contents, at the end of the process of the lyophilization system, is evaluated by the percent water content which became the metric of interest for the deflection requirement. Water leaves the product through the process of the lyophilization system and the final product needs to be evaluated down to a 0.1% water content. The selected laser displacement sensor (described in greater detail in the sensing section) has a minimum resolution of 0.25 microns. To err on the side of caution it was assumed that the minimum resolution that could consistently be obtained would be 1 micron. It was also assumed that the final product weight would be approximately 1 g as is standard for similar lyophilization processes. In order to obtain a percent water content of the final product down to 0.1% of the product weight needed to correspond to an overall deflection of 1 mm between the initial state, with an aqueous solution, and the final state, with a solid containing small amounts of water. It is important to note that this is a deflection change between two states where the water content of the product is the only mass leaving the vial. The weight of the vial itself is not part of this calculation which is very useful as there is some variation between vials. An additional important parameter was that 6mm of deflection was required for an applied weight of 15 g (which includes the vial, vial contents, and cap).

Table 1: Process Metrics.

Detail	Value	Units
Total Mass at End of Process	16	g
Vial Mass	15	g
Dry Matter Mass	1	g
Percent Resolution of the Dry Mass	0.10%	[]
Mass Detected	0.001	g
Parts: 1 Part In	16000	[]

In the table above the process metrics are shown. This breakdown allows for the small amount of mass detected to be shown in context of the other values for the system.

1.1.1.4 Manufacturability

Because the weight-sensing subsystem was designed for a lyophilization system which usually are commercial scale machines it was crucial that the subsystem be manufacturable at a large scale. The prototypes described in subsequent sections were usually made with prototyping approaches such as 3D printing and hand bending spring. This would not be feasible for production of the full weight-sensing subsystem for the larger lyophilization system so special consideration was given to ensuring that the weight-sensing subsystem components could be manufactured and assembled at a large scale without unreasonable amounts of labor or time.

1.1.1.5 Sterility and Particulate Generation

The sterility and particulate generation of the lyophilization system and the weight-sensing subsystem in particular were of concern. In order to ensure that this subsystem was designed to meet current requirements the materials selected for use in this subsystem were already in use in similar lyophilization systems currently in use. This meant that the materials were known to work well in sterile environments (not releasing contaminants and able to survive steam cleaning). The subsystem was designed with special consideration to exclude or minimize rubbing or sliding interfaces which had the potential to generate particles.

1.1.2 Existing Sensor Review

Sensors which can read weight changes using deflection are fairly common and exist in many forms. Perhaps the most common is a load cell in which strain gauges translate deformation into electric signals. The deformation profile can be designed by designing the flexure to behave in a particular desired way. For example, the required resolution and reading range can drive the flexure design (Jocelyn Kluger, 2017).

As space is often limited the design of compliant components that have a small footprint but are compliant in specific directions and deflect in certain directions is another area which has current examples. One such example was the design of shamrock electrical contacts which utilized a small footprint of area but were able to achieve the desired deflection (United States of America Patent No. 5973394, 1999).

The particular geometry constraints of the larger lyophilization system meant that the weight-sensing method had strict limitations which prevented the use of current existing sensors. The designs explored for the weight-sensing subsystem were heavily influenced by the existing sensors and designs described above but were designed to fit the specific requirements of the larger lyophilization system.

2. Weight-sensing Deflection Subsystem Design, Fabrication, and Evaluation

The following sections illustrate the evolution of approaches for the weight-sensing subsystem. After the general design details the Bent Spring approach is presented. The Bent Spring approach is the design which was ultimately selected and met its performance requirements. It is presented first in the upcoming sections. The Bent Spring design was the last design in a series of approaches progressing through flat Triangle Flexures, Alternative Flexure designs, and Diaphragm designs. Each of the design approaches that preceded the Bent Spring design had performance and/or manufacturability concerns that eliminated them as viable options. However, each eliminated design did help to inform aspects of the successful Bent Spring design.

Vial Spacing General Design Geometry

While the general design requirements for the overall weight-sensing subsystem are described in the previous section there are also key vial spacing geometry requirements which persisted

through all of the weight-sensing subsystem approaches. This is because a series of vials were to be run through the lyophilization system together.

To begin, the weight-sensing subsystem holds the glass vials with product contents. The vials were packed in an array that allowed for maximized throughput while also ensuring the vials had sufficient distance between each other to prevent significant differences in the heat transfer experience of vials in the center of the array verse vials on the perimeter of the array. As will be seen below the final configuration selected had three columns of vials and five rows making up one array and a large number of arrays would be in the larger lyophilization system at once. A hexagonal close packed array structure was selected to optimize the surrounding space between each vial.

Retaining Posts

In the larger system there is a stage where the vials experienced crossflow which could potentially tilt or in an extreme case tip the vials over. To mitigate this risk vertical retaining posts mounted to the base whose sole purpose was to keep the glass vials from tipping were to be integrated into the weight-sensing subsystem architecture. The presence of the retaining posts would also help prevent uneven loading conditions on the springs which could result if the vial tipped. Potentially a severe enough uneven loading condition could damage the springs. However, in normal use the retaining posts would not make contact with the vials. Additionally, these retaining posts served as useful references for the laser displacement sensor as there would be no vertical displacement over time of these fixed posts and the posts could therefore act as a calibrating feature.

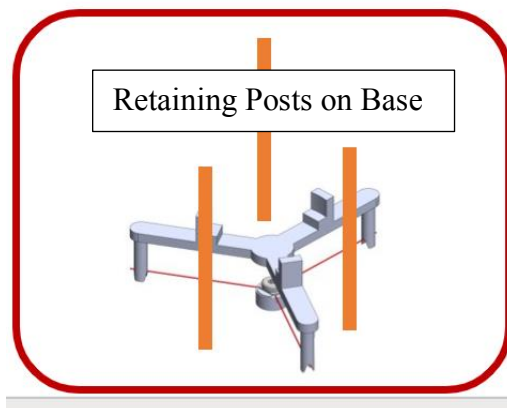


Figure 1: Retaining Posts.

The retaining posts shown in orange are mounted to the base and helped to ensure that the vial resting in the center of the posts could not tip over. The vial would contact at least one retaining post when tilting and not fully tip over.

Bent Spring

The Bent Spring design is the design which met all of the design requirements. Achieving sufficient deflection and having a design which is manufacturable at-scale were the two largest challenges which will be clear through later sections describing designs which did not meet all of the design requirements.

Initial design ideas were evaluated with the deflection calculation described below which allowed for approximate expected deflections to be calculated for the various design options. The calculations were then compared with simulation results and experimental results.

$$\delta_{\max} = \frac{Pa^2(3L-a)}{6EI}$$

δ_{\max} = maximum deflection [m]

P = applied force [N]

a = distance from mounting point [m]

L = total length of beam [m]

E = modulus of elasticity [Nm^{-2}]

I = area moment of inertia [m^4]

For the bent spring patterns the cross section of the deflecting beam was circular as wire stock was used for the beam. In the spring approaches, like that of the bent spring, where there was a straight section and arc section of wire the total beam length was the sum of the straight section and arc length.

2.1.1 Final Bent Spring Design

The Bent Spring design described in this section is the most current design that is intended for use in the lyophilization system. Additional validation and experiments with this design are ongoing at the time of writing. The final design presented here is a slightly revised version of the design which was prototyped and tested in the set of experiments described in the upcoming section.

The Bent Spring approach has three major components. The first is the vial holder which will hold the vial and rest on three springs. The wire springs are the next major component and have a specific geometry that wraps around the outer circumference of the vial with enough beam length to achieve the desired deflection. The wire springs are held by mounting posts which are themselves mounted to the radiation shield that is the lowest layer of the weight-sensing assembly and serves as the base. The radiation shield is used to reduce unintended heating from below the vial array. The three springs and contact locations between the vial holder and the springs allow for the assembly to be stable.

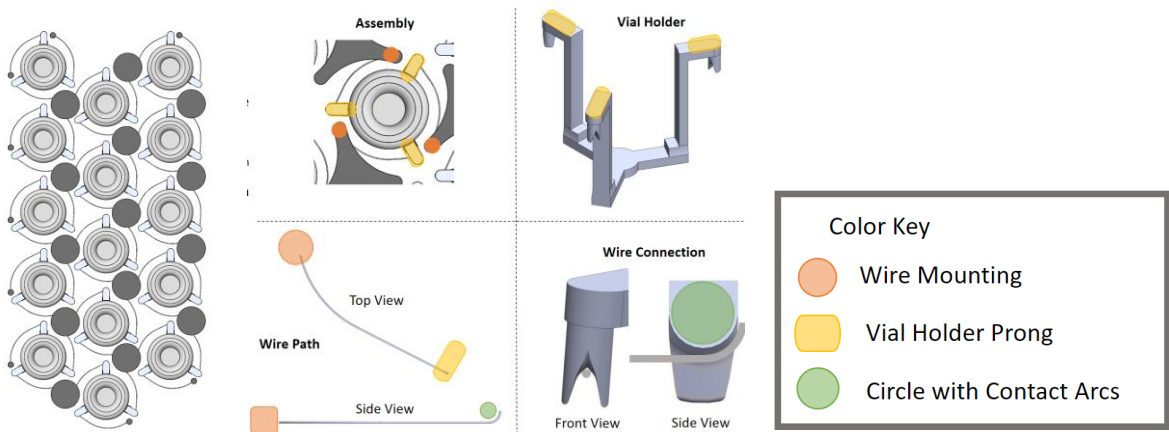


Figure 2: Bent Spring Layout.

The images above show the Bent Spring vial layout and the interfaces between the vial holder and the wire connections.

The vial holder has three prongs which rest on the springs. The given profile of the connection between the vial holder and the springs is designed to catch on the end of the wire so that the vial holder does not slide off the end of the wire and has a groove in which the wire sits so that

the wire and vial holder do not become disconnected. The vial holder will be an injection molded component for at-scale manufacturing.

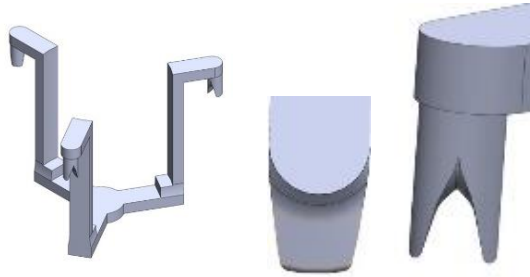


Figure 3: Vial Holder Wire Connection.

The vial holder is shown above with a side and front view of the wire and vial holder interface.

At scale for the full system the wire mounts (the component mounted to the base and holding the wires fixed) would be made up of two injection molded components, a washer, and a bolt. The standard wire mount would hold three wires but there would be additional versions of the standard post mount that only held two or one wire instead of the standard three. As can be seen by the top view in Figure 4 there were certain locations on the array which require 3, 2, or 1 wire to be supported at a particular location.



Figure 4: Wire Mounts.

From left to right: a top view of an array of Bent Spring designs, an exploded view of the wire mount, the wire mount, an experimental prototype of the Bend Spring wire mounts design. The two bottom components in the exploded view are the injection molded components. A washer and bolt are added on top of the injection molded components.

The lower interface which served to clamp the wires had a hexagon feature in the injection molded component around which the top interfacing component for the clamp fits. This allows for the wire channels in the top and bottom components to line up. The channels themselves are just under a complete semicircle cross section on the top and bottom to allow for the wire to be held between the two injection molded components. The bottom of the mounting posts is a hexagon shape which is used to help locate the posts on the radiation shield base.

From the top view the wire profile had a section which was curved and a section which was straight. The overall length of approximately 30mm of this component yielded the sufficient deflection of 1mm between initial and final states (with full water content and with very little water content). The section of the wire that was straight could be converted to a curve to increase the overall beam length if the desired deflection value increased above 1mm. From the side view the wire has a tighter curved section at the end which interfaces with the vial holder. This curve is to ensure the vial holder does not slide off the end of the wire.



Figure 5: Wire Profile.

Left: A top view of the wire profile showing the curved section and the straight section. Right: A side view of the wire profile showing the tight curve at the end of the wire which interfaces with the wire holder.

2.1.1.1 Material Selection at Scale

In the manufactured weight-sensing subsystem the injection molded components would be made from a material that is known to be compatible with biologics, survives the temperature range, and does not release contaminants through off gassing. There are a variety of materials which can meet these requirements and are currently in use in lyophilizers or similar systems.

The other components in the weight-sensing subsystem will be made out of stainless steel. The material that was most difficult to select was the wire material. Ultimately [McMaster 9495K51 - Spring-Back Multipurpose 304 Stainless Steel Wire 0.009" Diameter] was selected as it gave the desired deflection while also being able to return to its initial state consistently when unloaded.

Titanium had been considered as a potential wire spring material based on its material properties and expected deflection. However, titanium wire was not easily found with a small enough diameter because the small nonuniformities in the material have a large impact on the performance of the wire at such thin diameters.

2.1.1.2 Evaluation

Experiments are ongoing with this design but the deflection requirement (1mm of deflection change between the initial and final conditions) should be met as the current experimental setup and design is very similar to the prototyped design described below which achieved sufficient deflection. The motivation for the changes to this design in comparison with the prototyped design below were driven by the desire to mount the wires more securely so that between loading and unloading cycles the wires would not move and the deflections are expected to be more consistent between runs as a result.

2.1.2 Prototyped and Tested Bent Spring Design

The prototyped and tested design of the Bent Spring approach was very similar to the final designed described above but with a less refined mounting of the wires to the mounting posts. In the prototyped design the wire springs were held between two washers that were clamped down by tightening a bolt. The washers were at the top of a stack of spacers which were stacked to obtain the desired height. The vial holder and wire profile are the same. For prototyping purposes the vial holder was 3D printed (Clear V4 Formlabs resin printed on a Form2 3D printer).

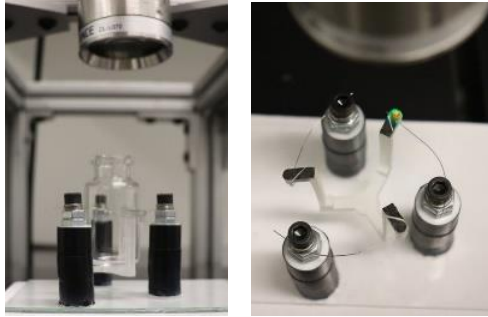


Figure 6: Bent Wire Experimental Setup.

The Bent Wire experimental setup is shown in the above images. In the image on the right the colorful mark on the uppermost vial holder prong is the Keyence laser displacement sensor spot. The Keyence sensor head is the silver cylinder show in both images.

The experimental results are shown below for experiments with the Bent Spring design. In these experiments a total of 3mL of water was added to the glass vial in 0.5mL increments where each additional 0.5mL was added droplet by droplet. There were pauses between each addition of 0.5mL which results in the stepped graphs shown below. As can be seen in these data the 1mm deflection change between initial and final conditions was met by this design. There was some variation between runs with regards to consistent initial (and therefore consistent final) overall deflection measurements, but the deflection change was encouragingly consistent. Between runs the entire 3D printed component was removed along with the glass vial and water contents.

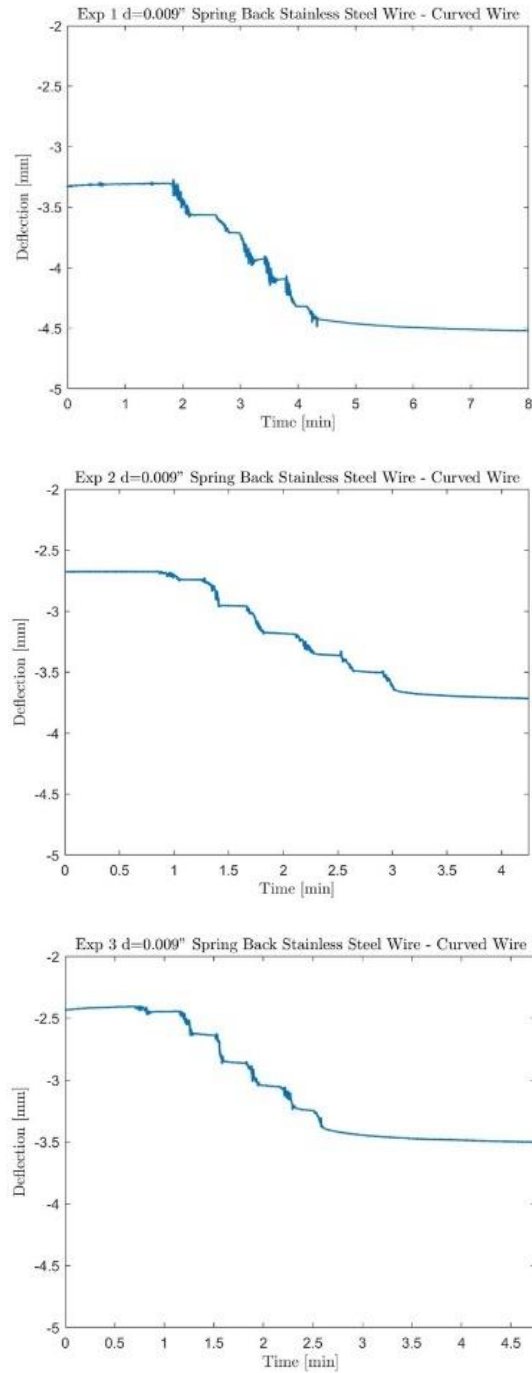


Figure 7: Bent Spring, Spring Back Stainless Steel Experimental Results.

The experimental results of three experiments with the Bent Spring design are shown above. As can be seen in the graphs the deflection change was more than the minimum deflection change threshold of 1mm.

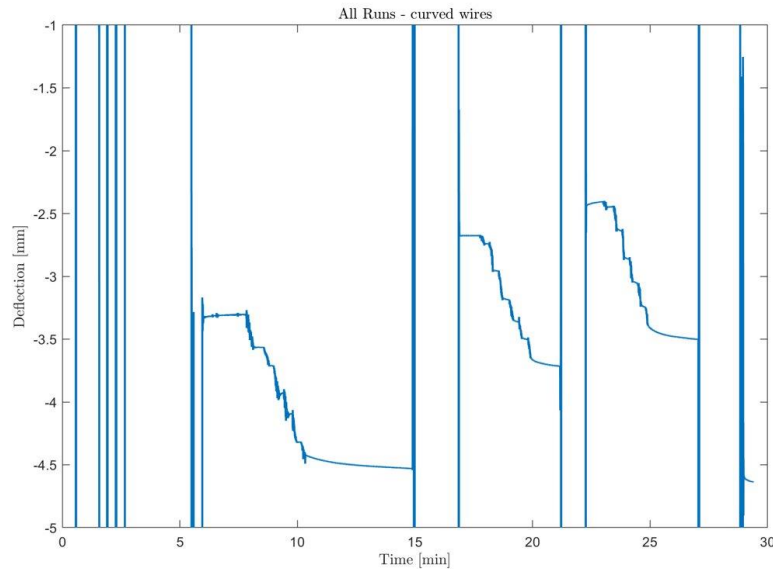


Figure 8: Bent Spring Design Experimental Results with Multiple Runs.

The figure above clearly demonstrates the varied initial start positions between runs. Subsequence prototypes with the final Bent Spring design should not exhibit this behavior to a similar degree.

As described previously, the above experiments were conducted with a Bent Spring design with the wires held between two washers. Because there was variation in the initial starting deflection between runs and there was some slight variation in the deflection change between runs the design was refined to that of the final Bent Spring design described in section 2.1.1. The final design has two injection molded components that will hold the wires more securely and should result in more consistent deflection results.

2.1.2.1 Straight Spring

Before the Bent Spring approach was the Straight Spring approach which yielded sufficient deflection (surpassing the 1mm deflection change threshold) but that was very unstable. This instability was a result of the center of mass of the system being above the wire spring connection points. This instability meant that the retaining posts were critical in keeping the glass vial upright even when there was no side loading on the vial. These experiments were conducted with

[McMaster 9495K51 - Spring-Back Multipurpose 304 Stainless Steel Wire 0.009" Diameter] as the wire spring material.

A major concern with relying on the presence of retaining posts for any loading on the springs was that contact between a retaining post and the vial meant that there was uneven loading, and the vial could "catch" on the posts and then "jump" instead of having a continuous deflection. The stability concerns and the desire to avoid contact with retaining posts for conditions outside of side loading led to the Bent Spring design described earlier which did not have these features.

The Straight Spring Design is shown below and held the three separate wires in place between a machined nut/spacer and a clipped washer. The clipped washer fit in with the machined nut/spacer to prevent the washer or nut/spacer from twisting while the bolt was being tightened. This enabled the straight wire springs to remain in their intended position through the bolt tightening.

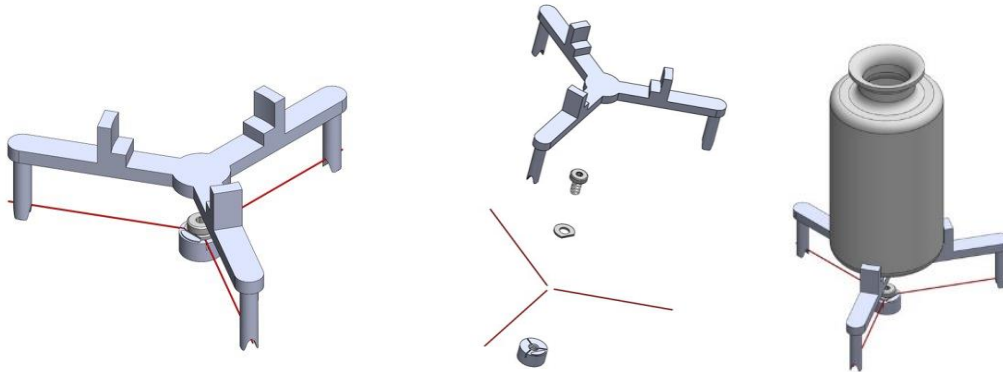


Figure 9: Straight Spring Design with Low Mounting.

The Straight Spring design shown above is an assembly (from bottom to top) of a machined nut/spacer, three straight wire springs, a clipped washer, a bolt, and the vial holder.

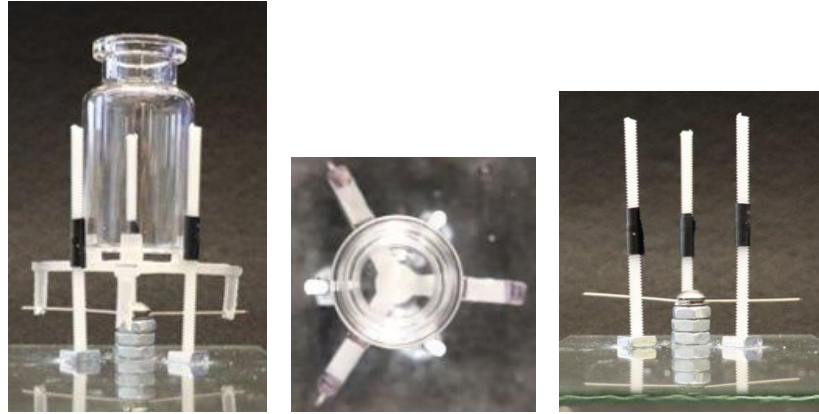


Figure 10: Straight Spring Design with Low Mounting Experimental Setup.

In the images above the experimental setup for the Straight Spring design is shown. The wire shown in the images was much thicker than the wire that was eventually used and yielded sufficient deflection.

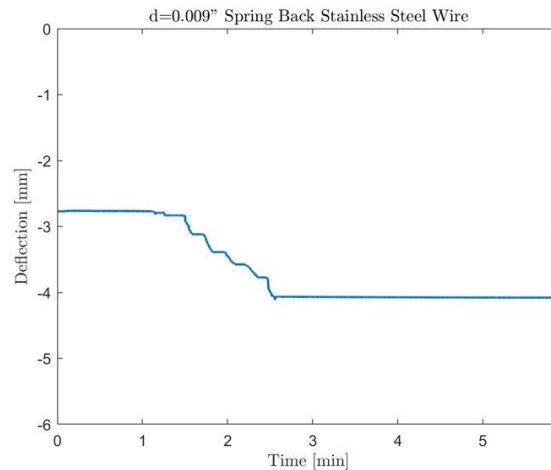


Figure 11: Straight Spring with Low Mounting Experimental Results.

As shown in the figure the deflection change between the initial and final loading conditions was greater than the 1mm threshold. Unfortunately, the instability of this design disqualified it despite achieving sufficient deflection change.

In the Straight Spring prototyping approach three wires were clamped between two washers below the base of the vial because this option was quicker to prototype than a machined nut/spacer. The table below shows the experimental and predicted changes in deflection for various wire diameters. This chart clearly shows that with thin enough wire diameters to obtain a predicted change in deflection greater than 1mm the experimental results showed that the wire would yield. These experiments were conducted with [McMaster 9882K13 - Round Bend-and-Stay Multipurpose 304 Stainless Steel Wire of various diameters] and with various prong lengths. Because of the instability there were also more cases of very uneven loading of wire springs which could also help explain the prevalence of yielding if the loading on a wire was substantially more than expected and simulated. The experiments described below were conducted before the better [McMaster 9495K51 - Spring-Back Multipurpose 304 Stainless Steel Wire 0.009" Diameter] had arrived.

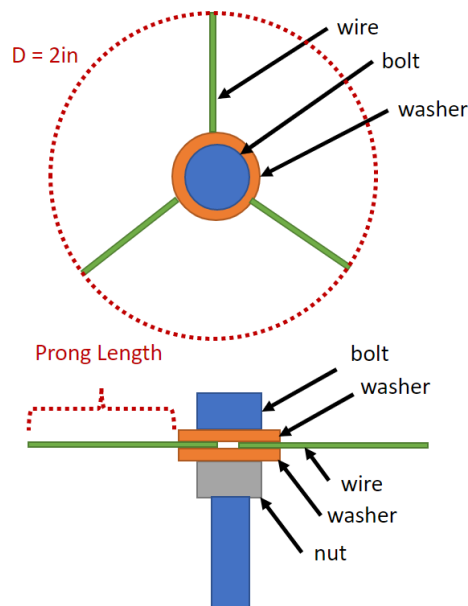


Figure 12: Straight Spring with Low Mounting Prong Length.

In the figure above the assembly holding the three straight wires is shown. The prong length and wire diameter were varied for this set of experiments.

Table 2: Straight Spring with Low Mounting Prong Length and Diameter Table.

Wire Diameter [mm]	Prong Length [mm]	Experimental Change in Deflection [mm]	Predicted Change in Deflection [mm]
0.23 [0.009in]	15.5	0.12	0.5
0.23 [0.009in]	18	yields	0.8
0.23 [0.009in]	22	yields	1.44
0.15 [0.006 in]	9	0.29	0.5
0.15 [0.006 in]	13	yields	1.5
0.15 [0.006 in]	17	yields	3.4

The table below is the summary of the experimental and predicted changes in deflection for a range of wire diameters and prong lengths. These experiments were conducted with [McMaster 9882K13 - Round Bend-and-Stay Multipurpose 304 Stainless Steel Wire of various diameters] which did not perform well but was the best option before the arrival of [McMaster 9495K51 - Spring-Back Multipurpose 304 Stainless Steel Wire 0.009" Diameter].

Having the straight wire springs radiating out from the center under the vial meant that there was a limit on the beam length imposed by the hexagon of useable space around each vial and even at the largest possible radius the overall assembly was extremely unstable. Simply adding

the vial to the assembly was enough to tilt the vial holder and vial enough to contact a retaining post.

In order to make the wire spring assembly more stable the points at which the vial holder made contact with the wire springs were moved upwards to be above the center of mass of the assembly. This meant that the assembly was more stable and also that the vial would not have the potential to tip over. In order to have this relationship between the contact points and the center of mass the spring wires themselves could no longer exist below the vial. The wire springs were moved up in relation to the vial and were mounted from mounting posts surrounding the vial instead of having a single mounting post below the vial's base holding all three springs.

When the wire springs were straight with no curvature in the top or side views the vial holder twisted with the addition of the vial enough to contact the mounting posts. It appeared that if the mounting posts did not prevent further motion that the vial holder would have continued to twist along the path of the straight wire springs and eventually slipped off the end of the wires.

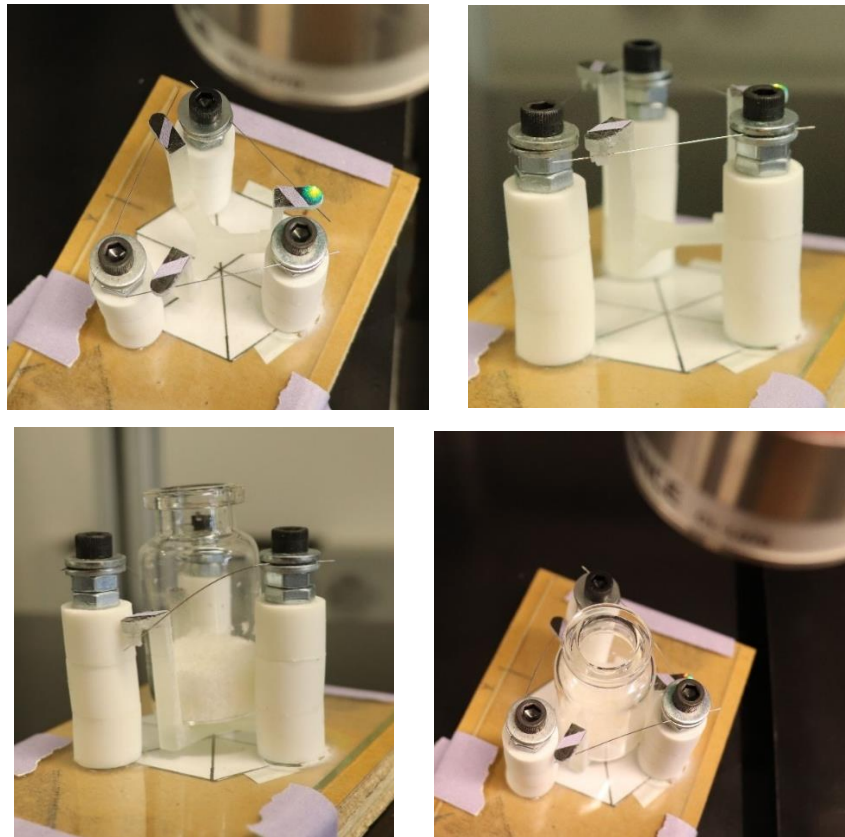


Figure 13: Straight Spring with High Mounting Experimental Setup.

The images above show the Straight Spring with High Mounting in an initial loading condition where the vial weight is at a maximum. The vial holder is contacting the mounting posts holding the wires because of rotation (clockwise in the images) of the vial holder.

The first approach to preventing the vial holder from rotating too much and slipping off the ends of the wire springs was to fix the connection point between the vial holder and the wire springs. This modification was done to the previous setup by adding a small amount of superglue to the connection points. This alteration did prevent excess twisting but also resulted in insufficient deflection (a deflection change between initial and final loading conditions of less than the 1mm minimum threshold). The deflection change in this case was about 0.5mm.

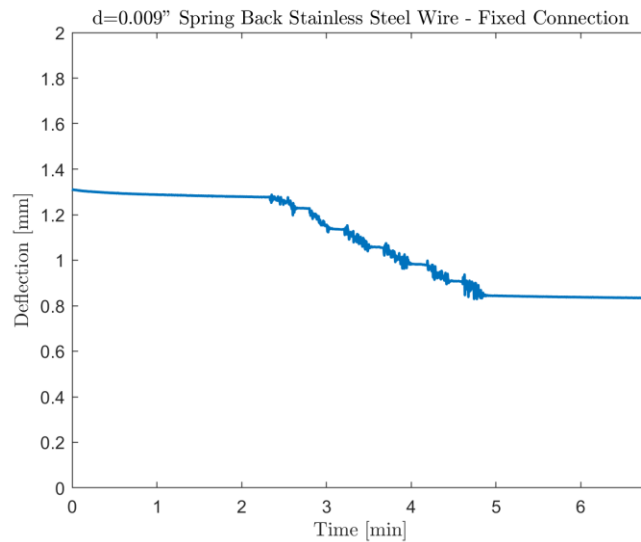


Figure 14: Straight Spring with High Mounting and Fixed Ends.

The insufficient deflection change is shown in the figure above. The fixed end configuration only resulted in a deflection change of only about 0.5mm between initial and final loading conditions. This was only about half of the required 1mm deflection change.

To prevent too much rotating of the vial holder on the wire springs but to allow for sufficient deflection change. A hard stop was introduced to the end of the wire springs. For ease of prototyping the initial hard stop design was simply a bent end of the wire. This modification allowed for sufficient deflection and did not have too much twisting. However, the initial right-angle bends were not well suited to the contact point profile between the vial holder and the spring wires so the vial holder itself "caught" and "jumped" on areas of the angled hard stop. This resulted in steps between incremental additions of 0.5mL of water to the vial that were less consistent. The six steps with the addition of 0.5mL of water each time do not follow a reasonable progression. For example, it can be seen that the 5th increment of water added had about three times as much deflection as the 4th or 6th increment of water added. This inconsistency was concluded to be due to the right angle hard stop at the end of the wire spring which is why in the Bent Spring design the end of the wire springs are curved. The curve prevented the vial holder from sliding off the wire springs while also allowing for a more continuous contact profile between the vial holder and the wire springs through the deflection of the wires.



Figure 15: Straight Spring with High Mounting and Right-Angle Hard Stops Experimental Setup.

The images above show the experimental setup of the Straight Spring design with high mounting and right-angle hard stops. The colored dot on one of the prongs of the vial holder in the lower left-hand image is the sensing spot for the Keyence laser displacement sensor.

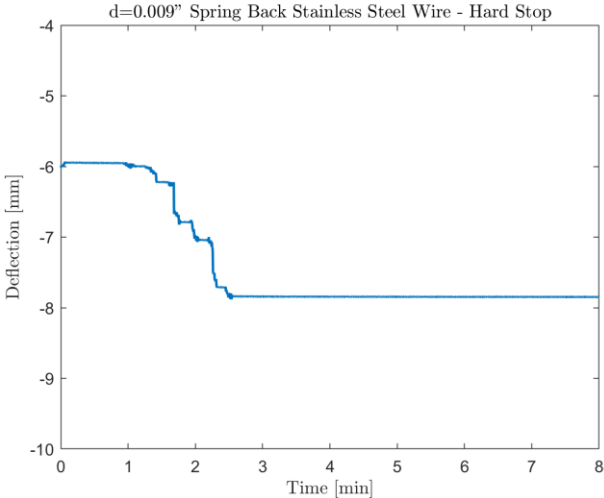


Figure 16: Straight Spring with High Mounting and Right-Angle Hard Stops Experimental Results.

The figure above shows the less distinct and less consistent steps which are a result of the vial holder catching on the right-angle hard stops and then slipping to a new location on the wire.

2.1.2.2 Full and Partial Loop Spring

Preceding both the Bent Spring design and the Straight Spring designs was an approach exploring more complex wire spring geometries. Ultimately these designs did not give sufficient deflection and also had a similar instability problem like the Straight Spring approach with the wires mounted below the base of the vial. In the full and Partial Loop designs below the center of mass of the assembly is above the connection points between the wire springs and the vial holder. There were hard stops to prevent too much deflection either from all the wires or from an individual wire or two from the set of three in the case of uneven loading. In many cases the hard stop was simply the base onto which the mounting posts were attached. The height of the mounting posts

allowed for desired deflection but would have the vial holder contact the base in the case of too much deflection. The figure below shows both the Partial and Full Loop Spring designs. The Partial Loop was one of three copies which would be arranged in a triangle around the vial while the Full Loop was one component that surrounded the vial.

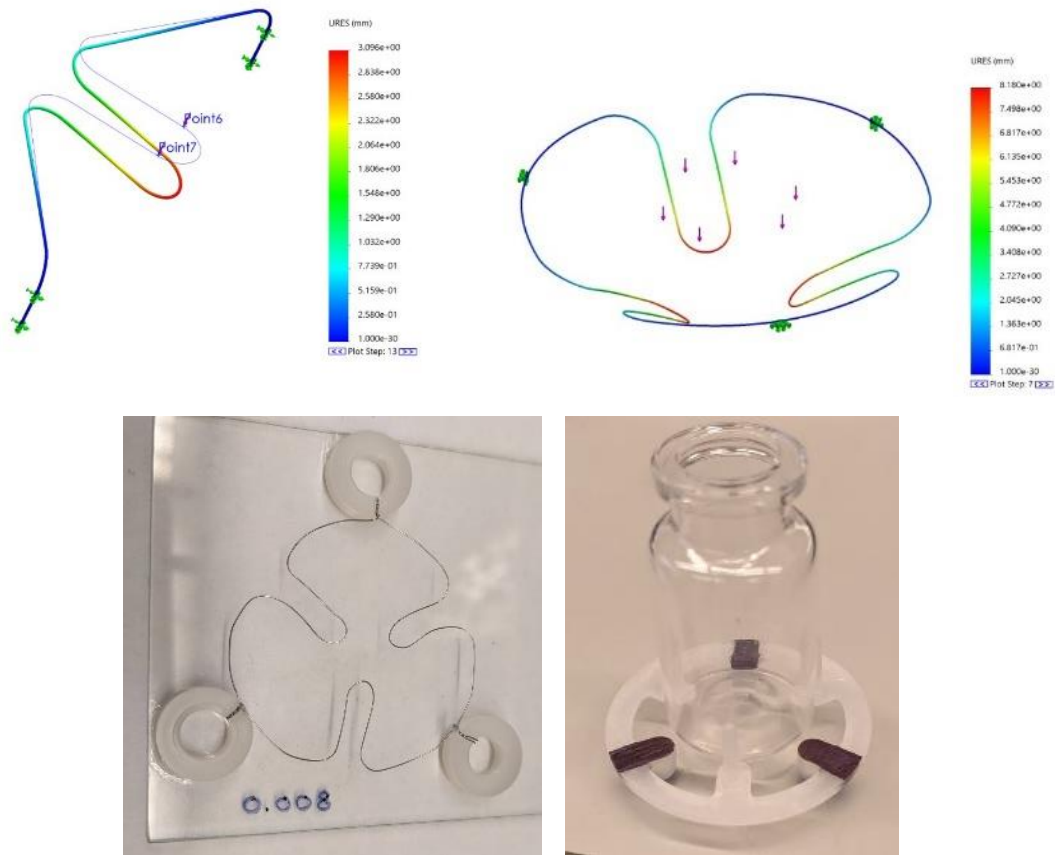


Figure 17: Full and Partial Loop Designs and Prototypes.

Clockwise from upper left: one Partial Loop component that would have been arranged in a triangle with two others to support the vial, one Full Loop component, a prototype of a full loop component, and the vial holder which sat upon the tongues extending towards the center of the vial in the Partial and Full Loop designs.

The vial holder and the spring profiles in the Full and Partial Loop designs were exploring the possibility of using a kinematic coupling to mount the vial holder on the spring. A kinematic

coupling approach was promising here because it had the potential for repeatable placement and location of the vial holder on the springs. Unfortunately, during experiments the wire used [McMaster 9882K13 - Round Bend-and-Stay Multipurpose 304 Stainless Steel Wire of 0.006in and 0.008in diameters] did not result in sufficient deflection without yielding and the deflection profiles showed continued deflection in steady states where the weight of the product was not changing which is likely the result of the material properties of the wire material used. These experiments were conducted before the [McMaster 9495K51 - Spring-Back Multipurpose 304 Stainless Steel Wire 0.009" Diameter] was obtained. Even when the more promising wire material was procured these spring design approaches were not revisited due to the instability concerns.

The Full and Partial Loop designs differ in that the Full Loop design is focused on utilizing torsion while the Partial Loop design is primarily in bending. Both the Full and Partial Loop designs take advantage of torsion and bending but they are more strongly utilizing one or the other. In both cases uneven loading led to tipping and in some cases bottoming out on the hard stop in one area that was unevenly loaded and deflecting more than intended. Once contact was made with a hard stop further deflection was not meaningful.

For prototyping the wire paths a fixture was built around which the wire would be wrapped. This bending was done by hand and with minor corrections also done by hand. The geometries of the wires for the Partial and Full Loops were fairly consistent. The same step-by-step protocol was followed for bending each wire. These wires were bent by hand for prototyping purposes but would be constructed through wire forming operations at scale.


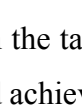
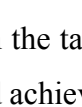
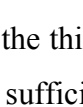
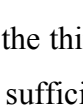
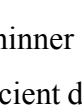
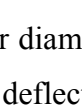


Figure 18: Wire Bending Template.

The image above is of the wire bending template that was used to form the Partial Loop spring patterns.

For both the Full Loop (primarily torsion) and Partial Loop (primarily bending) designs these two wires [McMaster 9882K13 - Round Bend-and-Stay Multipurpose 304 Stainless Steel Wire of 0.006in and 0.008in diameters] were used for prototyping the Full and Partial Loop approaches. Both gauges of wire resulted in insufficient deflection in the Full Loop design and the thinner wire yielded in the Partial Loop design and had insufficient deflection in the Partial Loop design. The simulation results indicated that the 0.006in diameter wire will be close to yield and this was supported with experiments as uneven loading (and presumably exceeding yield) resulting in yielding of the wire material. For prototyping the 0.008in diameter wire was less of a yield risk but the simulated deflection change was only 0.7mm which is below the minimum threshold of 1mm of deflection change.

Table 3: Summary of Full and Partial Loop Simulations.

Index	Spring Type	Spring Material	Spring Diameter	Maximum Deflection with 0.017N (min) --- 0.022N (max)	Deflection Difference	Maximum Stress with 0.017N (min) --- 0.022N (max)	Maximum Strain with 0.017N (min) --- 0.022N (max)	Deflection/ maximum stress ratio	Top View	Isometric Projection	Number of Parts
			[mm]	[mm]	[mm]	[N/m ²]	[]	[m ³ /N]			
1	Bending	304 stainless steel	0.15	6.52 --- 7.88	1.36	5.8*10 ⁸ --- 7.4*10 ⁸	2.2*10 ⁻³ --- 2.7*10 ⁻³	1.124*10 ⁻¹¹ --- 1.065*10 ⁻¹¹			3
2	Bending	304 stainless steel	0.20	2.42 --- 3.10	0.68	2.7*10 ⁸ --- 3.5*10 ⁸	8.0*10 ⁻⁴ --- 1.0*10 ⁻³	8.963*10 ⁻¹² --- 8.857*10 ⁻¹²			3
3	Torsion	304 stainless steel	0.15	6.79 --- 8.18	1.39	5.3*10 ⁸ --- 6.8*10 ⁸	1.9*10 ⁻³ --- 2.4*10 ⁻³	1.281*10 ⁻¹¹ --- 1.203*10 ⁻¹¹			1
4	Torsion	304 stainless steel	0.20	2.50 --- 3.19	0.69	2.3*10 ⁸ --- 3.0*10 ⁸	8.1*10 ⁻⁴ --- 1.0*10 ⁻³	1.087*10 ⁻¹¹ --- 1.063*10 ⁻¹¹			1
5	Torsion (corner for bolt)	304 stainless steel	0.15	6.67 --- 8.03	1.36	9.1*10 ⁸ --- 1.1*10 ⁹	2.8*10 ⁻³ --- 3.5*10 ⁻³	7.330*10 ⁻¹² --- 7.30*10 ⁻¹²			1
6	Torsion (corner for bolt)	304 stainless steel	0.20	2.44 --- 3.11	0.67	3.7*10 ⁸ --- 4.6*10 ⁸	1.1*10 ⁻³ --- 1.5*10 ⁻³	6.595*10 ⁻¹² --- 6.761*10 ⁻¹²			1

The table above summarizes the simulation results for the 0.006in and 0.008in wire. As can be seen in the table the thinner diameter wire had simulated results that would achieve a sufficient deflection change but was too close to yield. The thicker diameter wire was not as close to yield but was not simulated to achieve the sufficient deflection.

The experimental results for the Full Loop had less than half of the simulated deflection change. This meant that even the thinner diameter (0.006in) did not allow for the Full Loop design to achieve a sufficient deflection change of 1mm. Additionally, with both wire diameters the constant weight steps between additions of water droplets were not a consistent deflection. The deflection was increasing over time when the weight was constant. This was not acceptable for the subsystem performance and this material and design combination was disqualified.

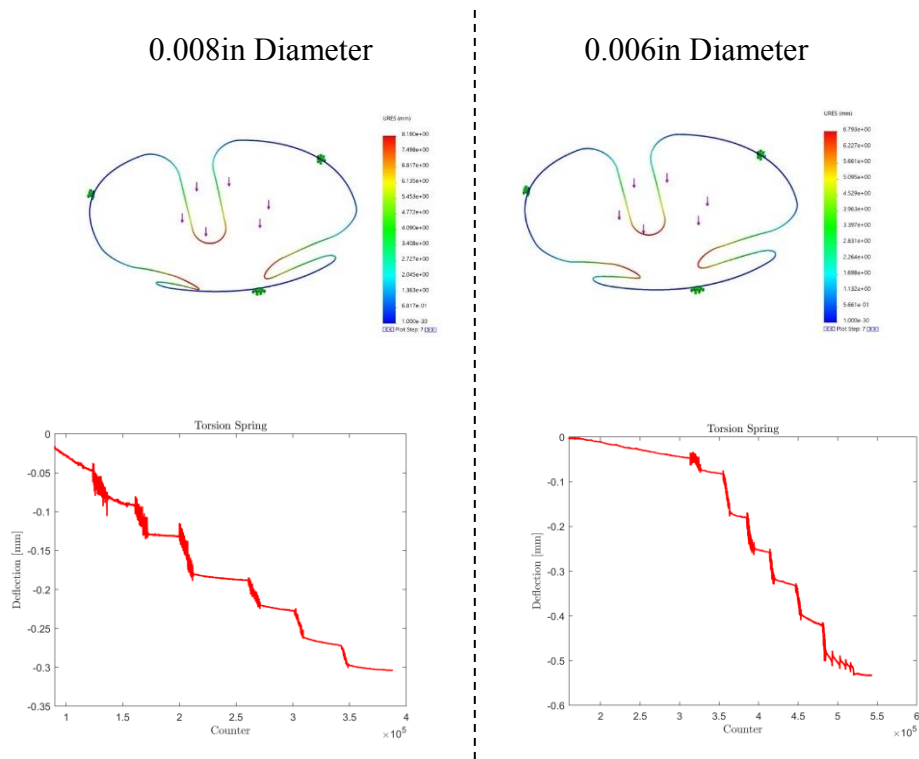


Figure 19: Full Loop Simulation and Experimental Results.

The figures above show simulations and experimental results for the Full Loop approach. The 0.008in diameter wire is shown in the left column and the 0.006in diameter wire is shown in the right column. Even with the thinner wire the deflection change was not sufficient. Additionally, the changing deflection readings during the constant weight steps disqualified this material and design as an option for the subsystem.

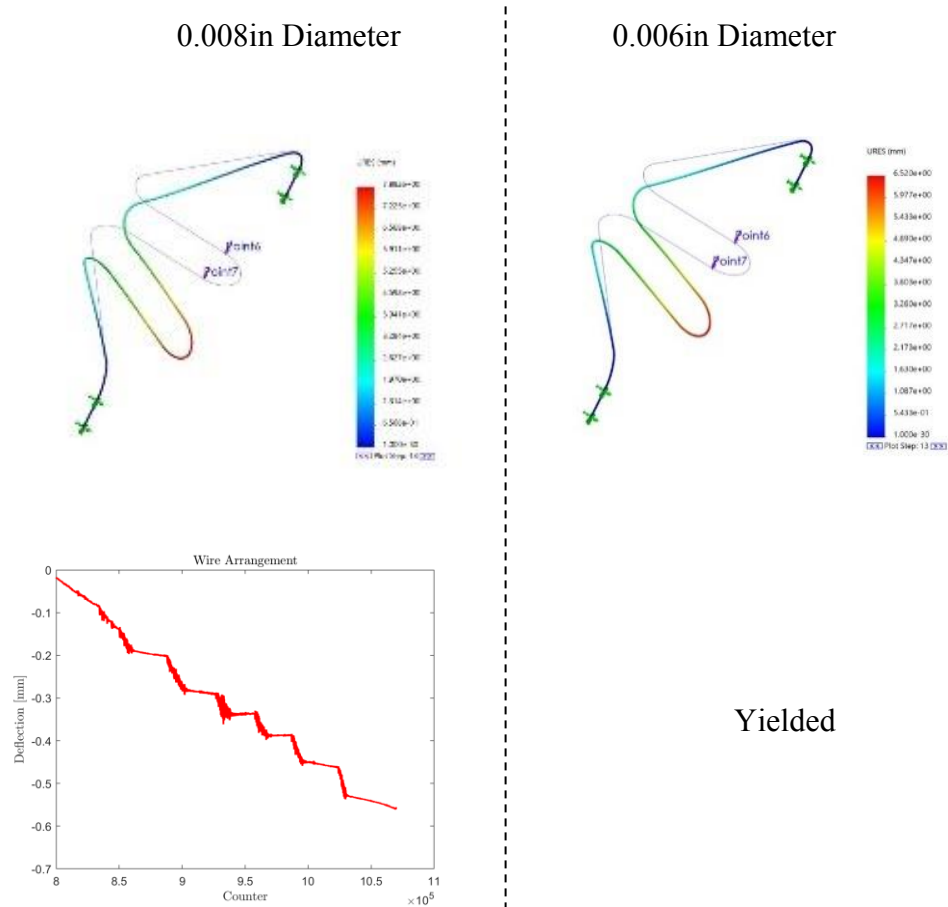


Figure 20: Partial Loop Simulation and Experimental Results.

The figures above show some simulated results and the experimentally collected data. The thinner of the wire diameters yielded and the thicker of the wire diameters did not yield but had considerable deflection changes over time when the weight supported was kept constant.

The experimental results for the Partial Loop with the thinner diameter wire agreed fairly well with the simulated results as there was a deflection change of almost 0.6mm seen experimentally when the simulations indicated there would be a deflection change around 0.7mm. However, this was not a sufficient deflection change and there were very pronounced changes in the deflection readings over time when the weight was held constant. For these reasons and the fact that the Partial Loop design was unstable this material and design combination was disqualified.

The Full Loop design was also appealing because all the wire supporting a single vial could be one component instead of the three separate components needed for the Partial Loop design. By having bolt and washer assemblies in the three corners of a Full Loop profile the single component could be effectively mounted. This mounting approach of clamping the spring wire between two washers using a bolt persisted through the Straight Spring designs. When prototyping a Full Loop could be connected using white brazing flux and silver solder.

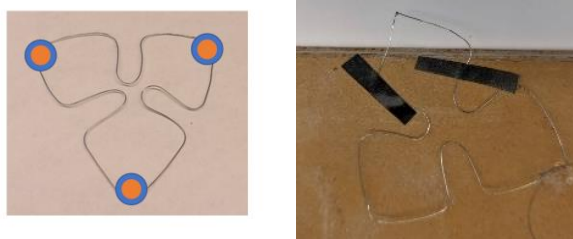


Figure 21: Full Loop Prototypes.

The images above show two prototypes of the Full Loop design. There were visible distortions in the geometry as these Full Loops components were bent to shape by hand.

Triangle Flexure

As mentioned previously the spacing of vials in the array was such that each vial would sit in the center of a hexagon of 2D space on the base of the array. A hexagonal close-packed arrangement was used and early in the design process there were concerns that a flat surface under the vial would not reflect enough radiation to sufficiently heat the vial. The primary source of radiative heating was coming from above the vial array which led to the "Tulip" designs which had angled triangles making up a cone shape below the vial in the hexagon of useable space. Later it was observed that a flat-bottomed base below the vials resulted in more heating of the product in the vial and the decision was made to proceed with a flat-bottomed base design with no angled surfaces. More details on the evaluations between the Flat and "Tulip" base approaches can be found in the section Tulip versus Flat Design. In both the Flat and "Tulip" designs the deflection was measured off of measurement posts attached to three of the triangles (cut to be flexures)

making up the surface below the vial. Ultimately both the "Tulip" and Flat Flexure designs were found to be impractical to manufacture which led to the decision to explore wire springs.

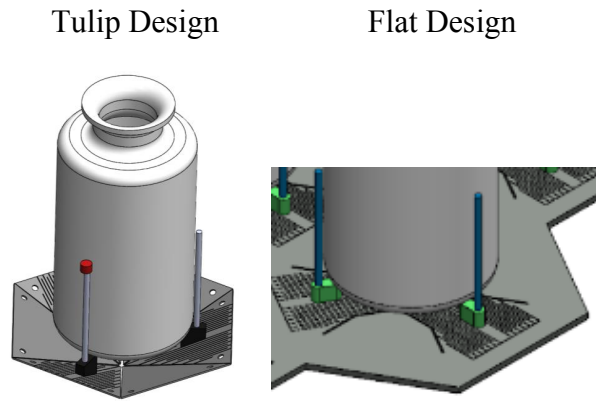


Figure 22: Tulip and Flat Flexure Designs.

The images above show the Tulip and Flat Flexure designs. Each had three reference posts attached to vial support pieces which were then in turn attached to the flexures.

Initial design ideas were evaluated with the deflection calculation described below which allowed for approximate expected deflections to be calculated for the various design options. The calculations were then compared with simulation results and experimental results.

$$\delta_{\max} = \frac{Pa^2(3L-a)}{6EI}$$

δ_{\max} = maximum deflection [m]

P = applied force [N]

a = distance from mounting point [m]

L = total length of beam [m]

E = modulus of elasticity [Nm^{-2}]

I = area moment of inertia [m^4]

For the flexure patterns the cross section of the deflecting beam was rectangular. And for most flexure patterns explored there was a symmetric beam path where two sections of flexure led from a mounting location to a single vial support. To account for this symmetry in the above calculations a factor of two was introduced so if a flexure's total beam length was 160 mm but it was symmetric so each half had 80 mm of beam length the 80 mm measurement was used in the calculations.

2.1.3 Design and Tulip Array

The "Tulip" design was motivated by early calculations which indicated that to achieve sufficient heating of the product in the vial radiation from the heated ceiling above the vials would need to be concentrated on the vials. From these early calculations the radiative heating the vial would receive from the walls and the heated ceiling without the introduction of a radiation concentrator (to help redirect more radiation to the vials) would not sufficiently heat the vials. Angled metal triangles were used to form a cone under each vial to act as a radiation concentrator.

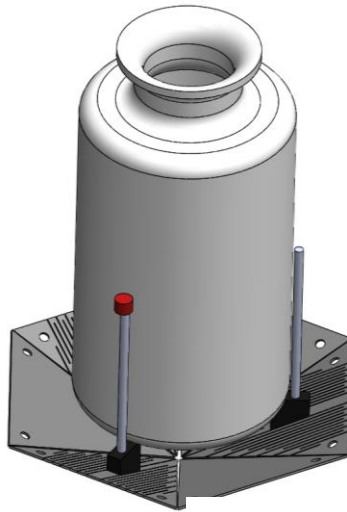


Figure 23: Tulip Flexure Design.

The stationary sides are marked with red and the flexure sides which deflect have the flexure pattern cut out of them.

2.1.3.1 Tulip Geometry

As described above the "Tulip" design has angled metal triangles forming a cone shape under each vial in the array to reflect radiation from the ceiling towards the vial's contents. The heating was concentrated on the lower third of the vial which is where the product is located. With the hexagonal close packed spacing a 2:1 ratio of collection area to focused vial area was achieved. The "Tulip" petals, or the individual metal triangles which made up the hexagon under the vial.

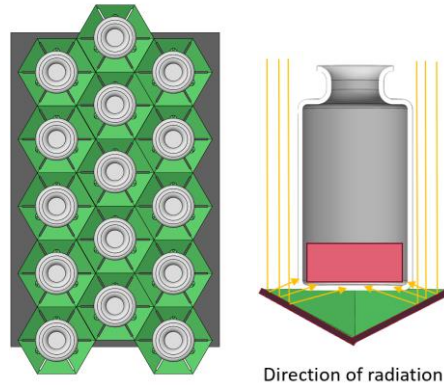


Figure 24: Tulip Flexure Radiation Concentrator.

The Tulip Flexure geometry was designed to direct radiation to the vial contents. The yellow arrows are the radiation paths to the red contents in the vial.

Three of the six petals which make up the cone beneath the vial are stationary and do not function as the flexures. The remaining three petals had patterns cut into their material which allowed for the petals to deflect with weight changes. These deflecting petals had support locations for the vial so that the vial was supported by the three flexural petals. The flexure petals and stationary petals alternate around the vial so that the vial is supported in three locations each at 120 degrees from the other support locations. Each flexural petal had a reference post that served two functions. The primary function of the reference posts was to help keep the vial vertical if the vial was tilting and the second function of the reference posts was to provide a surface from which to take deflection readings with the laser displacement sensor.

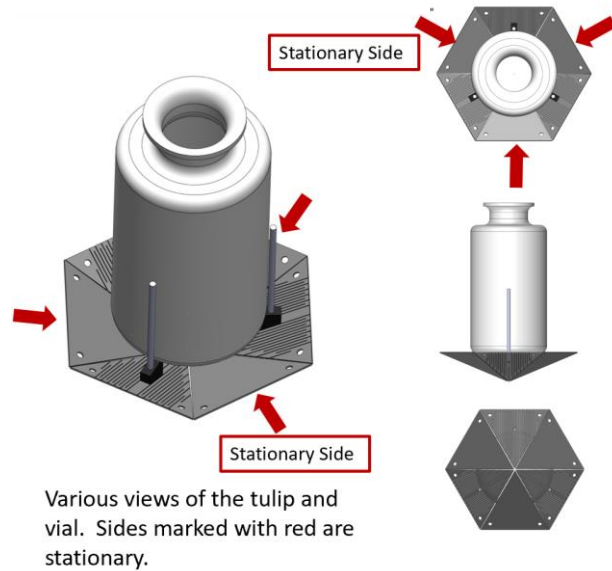


Figure 25: Tulip Flexure Stationary Sides.

The image above shows the stationary flexure sides with red arrows.

2.1.3.2 Flat Geometry

During preliminary experiments with vials and no "Tulip" geometry more heating of the vial product was observed than anticipated. This led to the question of whether or not the "Tulip" radiation concentrator was necessary and more fundamentally, whether a "Tulip" design or a Flat Base design would result in more heating of the vial contents.

If a Flat Base was sufficient then it would substantially reduce the complexity of the weight-sensing subassembly which would in turn decrease the cost and time to assemble. A Flat Base design would also allow for the possibility of integrating all the flexures into one piece. This flat design would take the Triangular Flexure components from the "tulip" design and lay them flat to make up the hexagon of space allocated for each vial. The vial supports and reference posts would be mounted directly to the single sheet base.

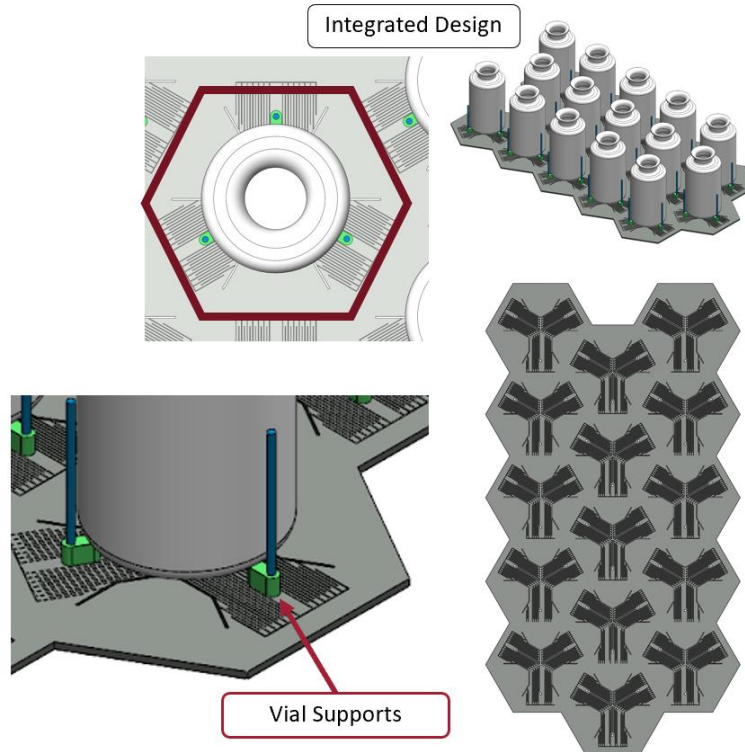


Figure 26: Flat Base Flexure Design.

The Flat Base Flexure Design has similar flexure cut paths to the Tulip design but the flexures are all integrated into one sheet.

2.1.3.3 Tulip vs Flat

In order to evaluate and compare the performance of the "Tulip" and Flat designs a set of experiments were conducted. The goal was to determine which option resulted in more heating of the vial product. The design with the greatest heating of the vial product would be the better option. Stainless steel sheets were used to construct prototypes of both designs. For comparison purposes the material used to make both prototypes were identical. Further down the road the particular emissivity's of various stainless-steel options (ranging from mirror finishes to black anodized) would be evaluated for the particular requirements of the larger system.

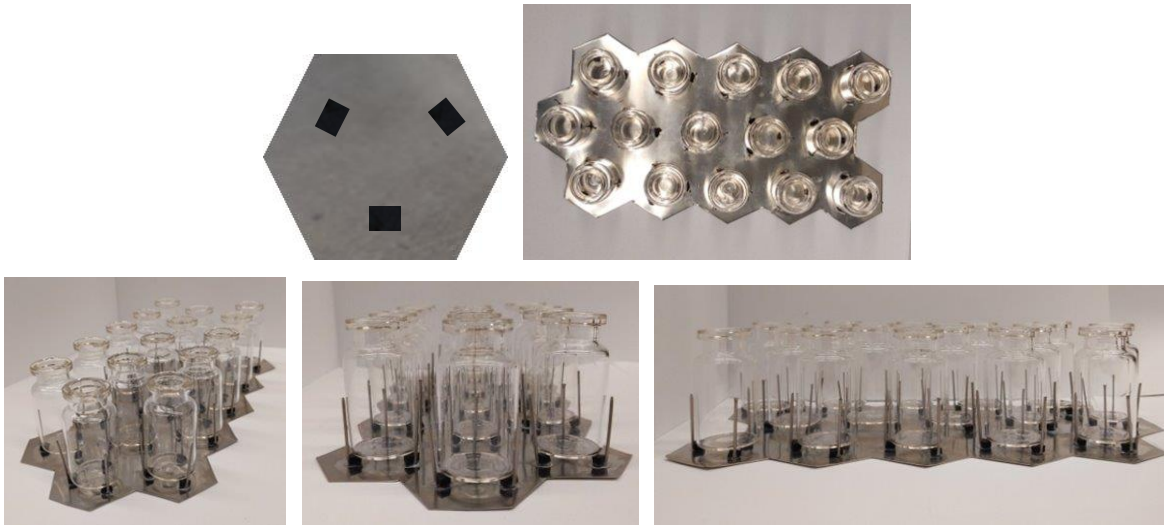


Figure 27: Flat Base Vial Array.

Various views of the Flat Base vial array are shown. The black components are the vial supports that keep the vials from resting directly on the base.



Figure 28: Tulip Base Vial Array.

Various views of the Tulip Base are shown above. The black components are the vial supports that keep the vials from resting directly on the metal triangles.

Experiments were run with both setups in a vacuum chamber with the conditions detailed below. Of particular note is the minimum vacuum chamber pressure of 130 Pa. This is a much higher pressure than the final system will be operating at and was a result of the limitations of the cold trap attached to the system.

Table 4: Tulip vs. Flat Experimental Conditions.

Experimental Conditions	Conditions
Maximum Heat Tape Temperature	60 degC
Maximum Vial Body Temperature	0 degC
Minimum Vacuum Chamber Pressure	130 Pa
Run time	90 minutes

Using a Two-Sample (assuming equal variances) t-Test with an alpha value of 0.05 there was found to be a statistically significant difference between the mean values of the Flat Base and "Tulip" Base designs. As can be seen from the plot below the Flat Base design resulted in more sublimation and therefore more heating of the product in the vials. The graph below shows the comparison between the Flat Base and Tulip Base in the amount of ice sublimated from vials.

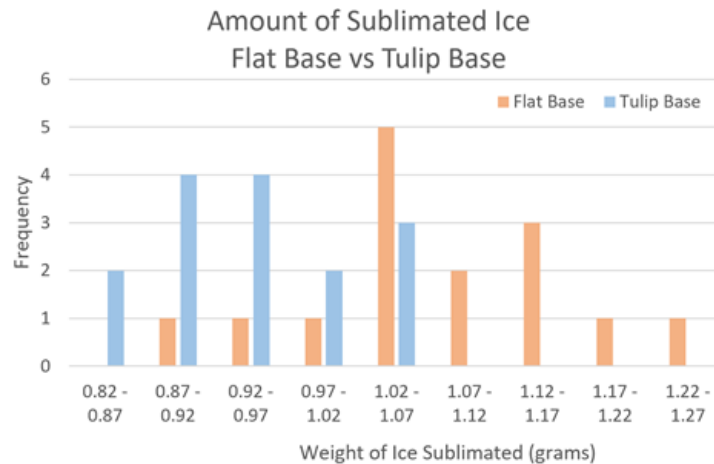


Figure 29: Comparison Between Flat Base and Tulip Base Sublimation.

The above figure shows the frequency and ice sublimated for the Flat Base and Tulip Base designs. It is clear that the Flat Base resulted in more ice sublimating from vials.

Additionally, temperature data was collected during these experiments. A ZnSe window in the side of the vacuum chamber and a FLIR camera allowed for temperature profile information to be obtained. For this set of experiments the FLIR results were not calibrated with a thermocouple or similar temperature measurement so the accuracy of the temperature measurements may be a few degrees off but the gradients in temperatures that can be seen from the Flat and "Tulip" designs demonstrate that the Flat Base design results in more uniform vial temperatures.

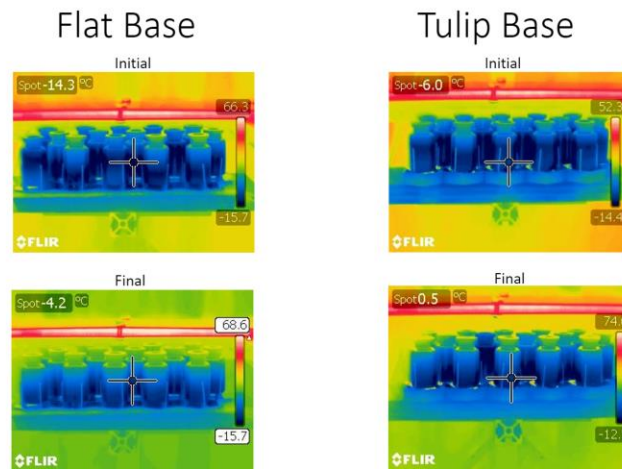


Figure 30: Flat Base and Tulip Base Thermal Images.

The Flat Base resulted in more uniform temperatures across the vial array. The Tulip Base had some noticeably colder vials in the center of the array at the end of the experiments.

The Flat Base yielded more sublimation which meant that the Flat Base design was selected to progress. As will be seen in the upcoming sections the infeasibility of manufacturing flexures with the required deflection change and footprint meant that despite the promising flat base design this was ultimately not a design that could be used in the larger system.

2.1.3.4 Modular Prototyping and At-Scale Manufacturing

Prototyping needed to precede the Flat and "Tulip" design option evaluation because prototypes were needed to run the experiments described above. For ease of experimentation a modular approach was taken so that various flexure patterns could be explored and swapped out. The "Tulip" design had six triangles (three stationary and three deflecting flexures) that would be cut for each vial while the Flat design had three deflecting flexures that would be cut and the rest of the hexagon was part of the single large sheet.

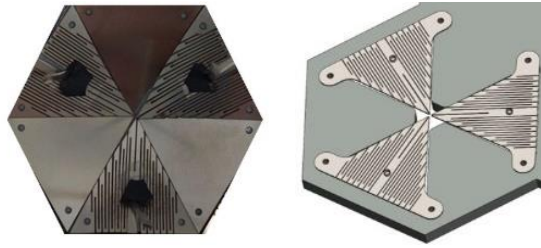


Figure 31: Modular Designs for the Tulip and Flat Flexure Designs.

On the left is a modular design for the Tulip design and on the right is a modular design for the Flat design.

The most challenging aspect of prototyping and manufacturing these assemblies was cutting the flexure pattern. Many patterns were explored but achieving sufficient deflection was not promising. Even with extremely tight cuts and long effective beam lengths the simulated deflections were not sufficient (simulations were conducted in SolidWorks 2019). The design that was manufacturable and the closest to giving the desired deflection is shown below and was selected to prototype. These prototypes were used to conduct experiments to study if the experimental deflection agreed with the simulated deflections which would mean these designs would not work in our system. If the experimental results showed more deflection than anticipated, then this design would have had potential to work in the larger system. As will be described in the next section the prototyped components agreed with the simulated deflection results which meant that this design was not viable in the larger system as there was not enough deflection change. The images below were of the flexures that were able to be prototyped and experimented with. These flexures showed that the effective beam length would need to be longer to give sufficient deflection and it was not possible to manufacture these Triangle Flexures with a greater effective beam length.

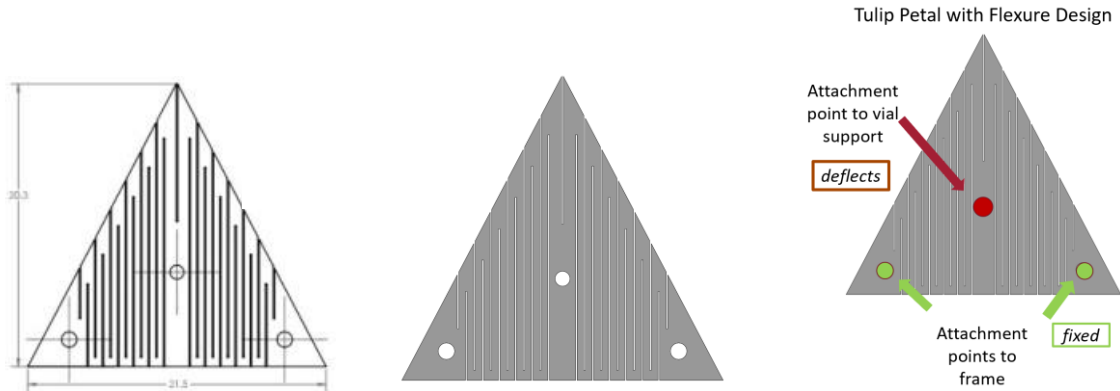


Figure 32: Tulip Petal Flexure Design.

The above images show the pattern for the Tulip petal flexure design.

There were a number of constraints on the Triangle Flexures and the manufacturing processes that meant one could not continue to modify the flexure design to achieve the desired deflection. There were tight constraints on the footprint of the triangles, the overall hexagon of space per vial, on material, on the material thickness, and on the spacing of cut paths. These hard limits meant that the design could not continue to be modified to increase the overall effective beam length which would have resulted in greater deflections.

There were three primary manufacturing methods for these Triangular Flexures that were explored. Water jetting, laser cutting, and chemical etching were all considered but ultimately not feasible for a flexure pattern that would yield sufficient deflection. The Triangular Flexures that were prototyped and yielded insufficient deflection were laser cut with a flexure pattern that was not expected to, and indeed did not, yield sufficient deflection but was manufacturable. The modifications to the Triangle Flexures that were needed to increase the effective beam length and therefore the deflection made the new designs un-manufacturable.

In order to fit in the geometry and be able to obtain sufficient deflection, the Triangle Flexures were to have the largest dimension on the Triangle Flexures be 21.5mm with a material thickness of 0.25mm and a cut width of 0.1mm. These Triangle Flexures needed to be made out of a non-magnetic stainless steel to be used in the larger system. With water jetting the cut width and material thickness requirements did not suit the flexure pattern. Laser cutting was considered but the features and cut paths were too close together and would result in distortion from

temperature gradients. The last option considered was chemical etching but the cut widths and the material thickness again would not work for the flexure pattern. Chemical etching had been very promising because with chemical etching the distortion and tapered cuts which can be found in laser cutting from heat buildup do not occur with the chemical etching process.

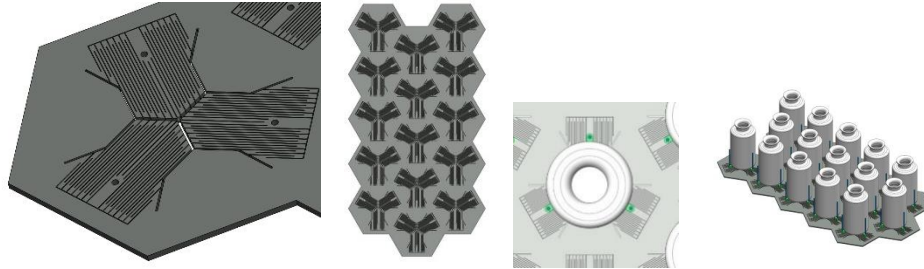


Figure 33: Ideal Flat Integrated Flexure Design.

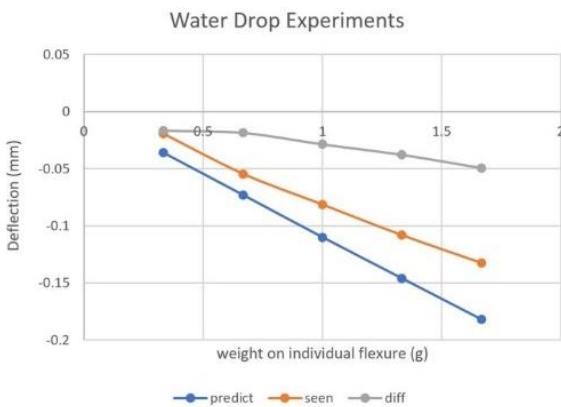
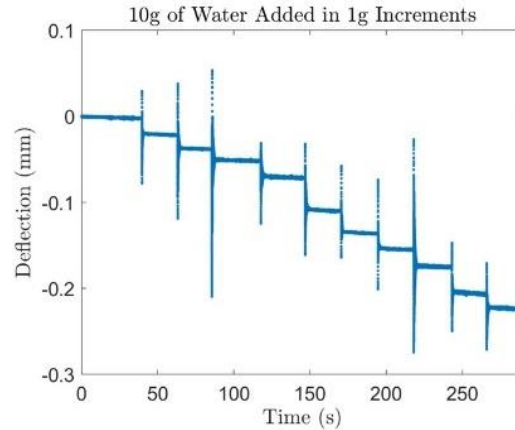
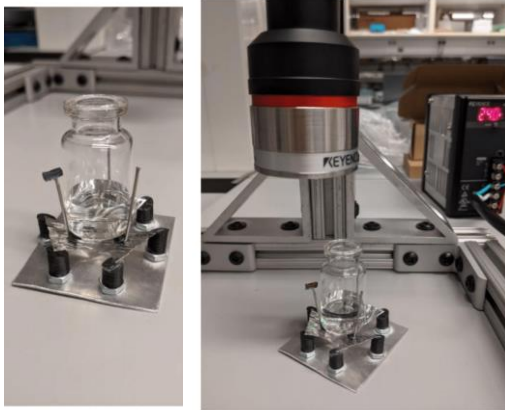
The above images show various views of the Flat arrangement of flexure cuts which were not manufacturable but would have allowed for all the flexures to be integrated into the base.

If any of the above manufacturing methods would have been feasible for cutting the flexure patterns desired there would have been the option to proceed with the flat design with fully integrated flexures. This design would have been very appealing because of the reduced part count and the reduced assembly time. Unfortunately, given that the necessary flexure paths could not be cut it was ultimately concluded that the flexure pattern required for the "Tulip" and Flat Flexure designs was not manufacturable.

2.1.3.5 Flexure Experimental Evaluation

This set of experiments was conducted with the Triangle Flexures which could be prototyped. These Triangle Flexures were not expected to yield sufficient deflection but were the manufacturable option with the longest effective beam length. Experiments were conducted to determine whether or not experimental values would agree with the simulated values. If the experimental values agreed with the simulated values, then it was to be concluded that this was not a viable design path to continue down.

Experiments were conducted by adding 10g of water to the vial in 1g increments. In the context of the larger system the deflection associated with approximately 3g of water is of interest but given the expected small deflections a larger amount of water was used to ensure the deflection change could be distinguished.



Weight on One Flexure	SW Deflection Estimation	Experimental Value	Difference
[g]	[mm]	[mm]	[mm]
0.333g	-0.036mm	-0.0194mm	0.0166mm
0.667g	-0.073mm	-0.0545mm	0.0185mm
1g	0.110mm	-0.0814mm	0.0286mm
1.333g	-0.146mm	-0.1082mm	0.0378mm
1.667g	-0.182mm	-0.1326mm	0.0494mm

Figure 34: Prototyped Flat Flexure Experiments.

Clockwise from upper left: images of the experimental setup of the Flat Triangle flexures, experimental results from the experiments adding 1g of water in 10 discrete steps to the glass vial, a graph comparing the predicted and observed deflection of the flexures, and the table from which the predicted and observed deflection chart was constructed.

The deflection threshold to meet was at least a 1mm deflection change between the initial and final conditions (when the product is fully wet and when the product is almost entirely dry). The weight change between these two conditions is approximately 3g. As can be seen from the data above there is not sufficient deflection change. This was to be expected as can also be seen above the simulation and experimental results agree. These results meant that the flexure pattern approach for both the Tulip and Flat designs were not feasible and new design approaches were considered. The immediate next step was to consider flexure pattern options which took advantage of more of the available space below the vials. Since the Flat design was seen to be promising there were no longer strict limits and triangular sections of a vial's hexagon to potentially be used for a flexure pattern. The alternative flexure patterns could spread out and take up a larger footprint than the Triangle Flexures and with a larger footprint the effective beam length could be increased while still working within manufacturing limits.

Alternative Flexure

Based on the Triangle Flexure's inability to deflect a sufficient amount other options for flexure patterns were explored. Since the manufacturing limits were fixed and not a variable that could be changed the best option for obtaining more deflection and a longer effective beam length was to adapt the flexure pattern. The encouraging results which had shown the previous flat design with the Triangle Flexure resulted in more sublimation and more uniform heating allowed for the flexure pattern to extend beyond its previous triangle limitations.

2.1.4 Design

Many different flexure patterns were explored with the new limitation that each flexure pattern should take up only one third of the full hexagon shape. This doubled the available surface area for a flexure pattern.

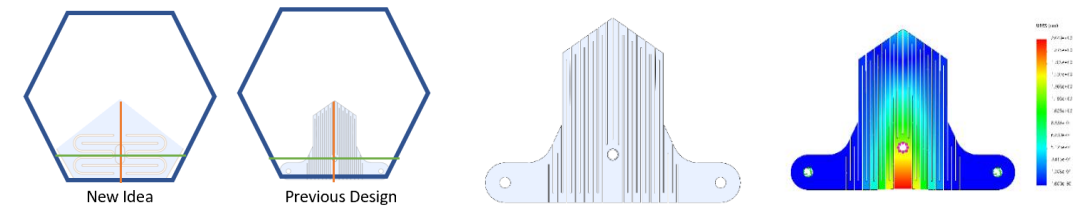
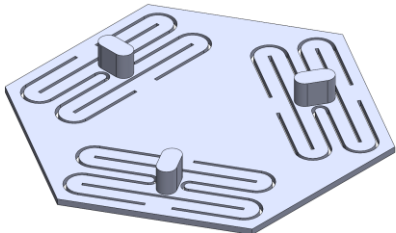
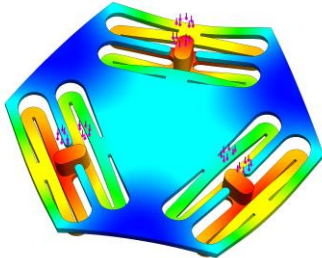
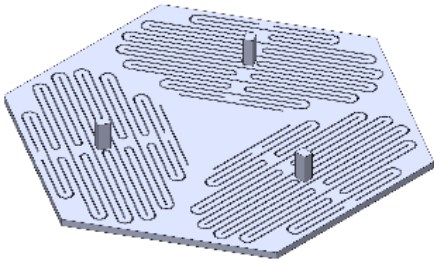
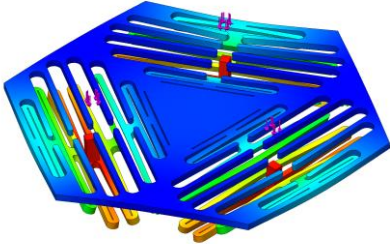
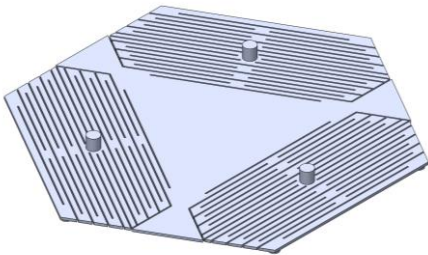
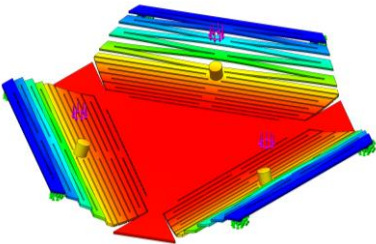


Figure 35: Alternative Flexure Patterns.

The above images show Alternative Flexure designs which take advantage of the additional available area beneath the vials.

Below is a table of flexure patterns for which simulations were run to determine if there would be sufficient deflection. For these designs it was assumed that the minimum beam width would be 0.35mm, the minimum cut width would be 0.1mm (laser cutting), and the minimum material thickness would be 0.25mm stainless steel. Unfortunately, none of these designs resulted in sufficient deflection.

Table 5: Alternative Flexure Patterns and Simulated Deflection Changes.

Index	Model Pattern	Simulations	Deflection Change [mm]
1			0.00369
2			0.0286
3			0.02

The above table displays some of the Alternative Flexure patterns explored. None of these flexure patterns were able to achieve the minimum required change in deflection of 1mm.

Diaphragm

After the manufacturing challenges with the flexure designs, a design was sought for a component that would deflect with a weight change but that would also be manufacturable and

ideally be prototyped by adapting a current off-the-shelf component. Diaphragms like those commonly found in small speakers were the next design option explored.

Initial design ideas were evaluated with the deflection calculation described below which allowed for approximate expected deflections to be calculated for the various design options. The calculations were then compared with simulation results and experimental results.

$$y = \frac{3T(1-\mu^2)Pa^4}{16Eh^3}$$

In the above equation T is a coefficient of reduction defined as:

$$T = \frac{y}{y_0}$$

y = corrugated diaphragm deflection [m]

y₀ = flat diaphragm deflection [m]

P = Pressure [Nm⁻²]

h = thickness [m]

a = radius of diaphragm [m]

E = modulus of elasticity [Nm⁻²]

r = radial distance [m]

μ = Poisson's ratio []

(Giovanni, 1982)

2.1.5 Design

Two approaches were taken to investigating Diaphragm designs. The first was to purchase standard stainless-steel Diaphragms and alter them to achieve sufficient deflection. The second was to design a corrugated Diaphragm that would be injection molded for the larger system but that would be 3D printed in an approximate material for prototyping.

2.1.5.1 Standard Component Approach

A Diaphragm design was promising because small metal Diaphragms are extensively characterized and very commonly found in electronics components. This meant that we could get a great deal of information on the manufacturing capabilities for similar components and that there

were off-the-shelf options which could be prototyped with. The major challenge was that the magnitude of deflection for corrugated Diaphragms is usually less than 0.127mm (Giovanni, 1982). In order to achieve more deflection design options were explored that were corrugated Diaphragms with large cutouts to give more deflection.

In exploring the corrugated Diaphragm design options many profiles of Diaphragms and modifications were run through SolidWorks simulations to determine how much deflection could be anticipated. The following tables are a summary of a selection of diaphragm design and a table of the simulation results for standard stainless-steel Diaphragms. As the second table shows none of the designs and alterations yield the sufficient deflection change of 1mm between the initial and final loading conditions (where the initial has the full water content, and the final condition has very little to no water content).

Table 6: Diaphragm Images and Simulations.

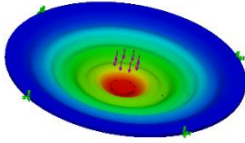

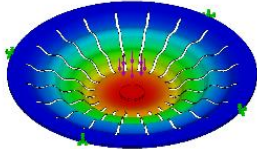
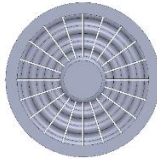
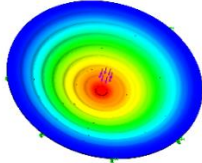

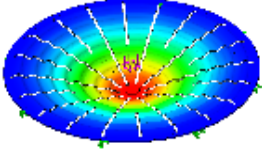

Name	Incisions	Cut Center		
HSLP1.00 0-TAB-B	no	no		
HSLP1.00 0-TAB-B	yes	no		
HSLP2.00 -TAB-B	no	no		
HSLP2.00 -TAB-B	yes	no		

Table 5 shows a small selection of the Diaphragms which were run through Solidworks simulations to obtain deflection estimates.

Table 7: Diaphragm Simulation Results.

Source	Name	Force Applied (N)	Max Deflection (mm)	Incision	Carved Center	Deflection Change (mm)
A	HSLP1.000-TAB-B	0.103	0.00297	No	No	
	HSLP1.000-TAB-B	0.132	0.00381	No	No	
						0.00084
	HSLP1.000-TAB-B	0.103	0.0248	Yes (20)	No	
	HSLP1.000-TAB-B	0.132	0.0318	Yes (20)	No	
						0.007
	HSLP1.000-TAB-B	0.103	0.0252	Yes (20)	Yes	
	HSLP1.000-TAB-B	0.132	0.0322	Yes (20)	Yes	
						0.007
B	HSLP1.500-TAB-B	0.103	0.00432	No	No	
	HSLP1.500-TAB-B	0.132	0.00555	No	No	
						0.00123
C	HSLP2.000-TAB-B	0.103	0.0075	No	No	
	HSLP2.00-TAB-B	0.132	0.0096	No	No	
						0.0021
	HSLP2.000-TAB-B	0.103	0.117	Yes (20)	No	
	HSLP2.00-TAB-B	0.132	0.150	Yes (20)	No	
					0.033	
D	Welch Allyn	0.103	0.00526	No	No	
	Welch Allyn	0.132	0.00674	No	No	
						0.00148

The above table is a summary of simulation results for a variety of diaphragms both standard and modified which showed that none of these options achieved sufficient deflections.

As is shown above none of the standard stainless steel Diaphragm options yield sufficient deflection. Additional materials beyond stainless steel were explored as a potential material from which to make the Diaphragms.

2.1.5.2 Injection Molding and 3D Printing Approach

As there were no standard stainless steel metal Diaphragms that would yield sufficient deflection change in this weight-sensing subsystem additional approaches and materials were investigated for creating corrugated Diaphragms.

On a prototyping scale these Diaphragms would be 3D printed while at a manufacturing scale these Diaphragms would be injection molded. Due to the strict sterility and biologics compatibility requirements of the larger system the materials explored for potential Diaphragm materials were those which already were approved for similar systems or materials which were very close in material properties to those already approved.

Table 8: Potential Injection Molding Materials.

Material	Current Form
bromobutyl rubber	West Lyophilization Stopper
Chlorobutyl rubber	Grainger Stopper
Butyl rubber	Capitol Scientific
Butyl-Isoprene	Capitol Scientific
Halobutyl	Capitol Scientific
chlorobutyl-isoprene	Wheaton – Capitol Scientific
HDPE (High-density polyethylene)	-----
PEEK (Polyether ether ketone)	-----

The above table lists potential injection molding materials which could be used to make the Diaphragm design. The options which have a company in their "current form" column were found to be the materials used in a lyophilization cap or stopper made by the company listed.

To begin, the most promising corrugated Diaphragm design from the standard options (HSLP2.000-TAB-B) was run through deflection simulations in SolidWorks using some of the common materials used in similar systems. The table above lists common materials that are already used in similar systems as well as HDPE and PEEK which were recommended as additional materials that could likely obtain approval for use in a pharmaceutical system such as this.

Table 9: Diaphragm Simulations with Injection Molding Materials.

Diaphragm Design	Material	Force Applied (N)	Max Deflection (m)	Deflection Change (mm)
HSLP2.000-TAB-B	Butyl, bromobutyl, chlorbutyl	0.103	0.702	
HSLP2.000-TAB-B	Butyl, bromobutyl, chlorbutyl	0.132	0.899	0.179
HSLP2.000-TAB-B	Butyl-isoprene, chlorobutyl-isoprene - ISOPRENE	0.103	0.0504	
HSLP2.000-TAB-B	Butyl-isoprene, chlorobutyl-isoprene - ISOPRENE	0.132	0.0646	0.0142
HSLP2.000-TAB-B	HDPE (High-density polyethylene)	0.103	0.9923	
HSLP2.000-TAB-B	HDPE (High-density polyethylene)	0.132	1.168	0.1757
HSLP2.000-TAB-B	PEEK (Polyether ether ketone)	0.103	0.317	
HSLP2.000-TAB-B	PEEK (Polyether ether ketone)	0.132	0.399	0.082

The above table show the simulation results for the deflection of the most promising Diaphragm design with a range of potential materials. As can be seen from the chart there is still no option which achieves the required 1mm deflection change.

For ease of prototyping HDPE was selected as the material to use as a reference for prototyping. Despite not having the greatest deflection change it came in as a very close second and is substantially easier to prototype with than bromobutyl or chlorbutyl.

The table below took the HSLP2.000-TAB-B geometry from the standard corrugated Diaphragm but altered the material thicknesses and assumed that the material was HDPE. This adaptation was done because the material thickness of the standard corrugated Diaphragm was that of a stainless-steel sheet which was too thin to injection mold.

Table 10: HDPE Diaphragm Simulation Results.

Material	Description	Thickness	Force Applied (N)	Displacement (mm)	Change in Displacement
HDPE	Solid disk	1mm	0.103	0.0074	
HDPE	Solid disk	1mm	0.132	0.0095	0.0021
HDPE	Solid disk	0.5mm	0.103	0.0528	
HDPE	Solid disk	0.5mm	0.132	0.0677	0.0149
HDPE	4 prong wheel	0.25mm	0.132	0.751	0.072
HDPE	3 prong wheel	0.5mm	0.103	0.460	
HDPE	3 prong wheel	0.5mm	0.132	0.532	0.072
HDPE	3 prong wheel	0.25mm	0.103	0.784	
HDPE	3 prong wheel	0.25mm	0.132	0.866	0.082

The above table shows the simulation results of various HDPE Diaphragm designs all of which again, did not achieve the 1mm minimum change in displacement.

Because the change in displacement in the previous table was still not at the 1mm deflection change threshold additional geometries of the corrugated Diaphragm were explored with HSLP2.000-TAB-B still serving as the base geometry. Incisions were made, the center was cut out, and small cuts made tapered beams on the end of which the vial would rest. These modifications were added to further modify the design in an effort to increase deflection.

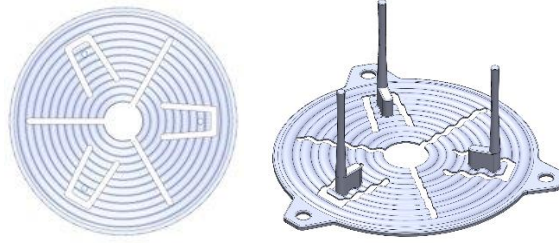


Figure 36: Modified Corrugated Diaphragm Design.

The above corrugated diaphragm design introduced incisions and tapered beams to increase the deflection achieved during loading.

In an additional step to take fuller advantage of the hexagon of space allocated to each vial the Diaphragm geometry was adapted to be a hexagon. Additionally, a second vial holder component was designed to interface with the Diaphragm. This allowed for the material thickness of the corrugated Diaphragm to be much more uniform (which allows for easier injection molding and 3D printing) and also allowed the vial holder component to be injection molded separately and out of a different material if needed.

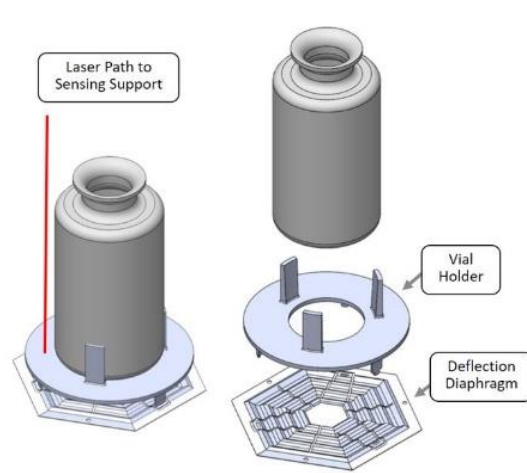


Figure 37: Hexagonal Diaphragm Design.

The image above shows the Hexagonal Diaphragm design with the separate vial holder which interfaces with the diaphragm below.

The following tables summarize the various designs that were experimented with for a hexagonal Diaphragm 3D printed by BMF [Boston Micro Fabrication] with their RG Resin because this material was the closest in material properties to HDPE, was bio compatible, and did not uptake water.

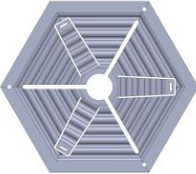
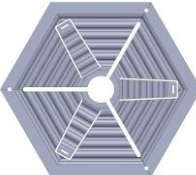
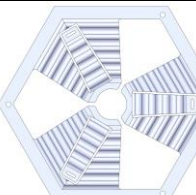
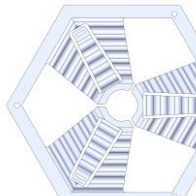
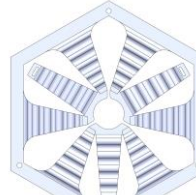
As can be seen in the tables below there were a few designs which simulations indicated would reach the 1mm deflection change threshold.

Table 11: BMF 3D Printed Diaphragm Simulation Results.

Material properties: https://bmf3d.com/materials/					Breaking Strength is 77.7 MPa		
ID	File Name	Material	Thickness [mm]	Force Applied [N]	Max Deflection [mm]	Def Change [mm]	Max Stress [Mpa]
A	linear_hexagon_V7_a	BMF-RG	0.3	0.103	2.367		
A	linear_hexagon_V7_a	BMF-RG	0.3	0.132	2.997	0.63	4
B	linear_hexagon_V7_a	BMF-RG	0.25	0.103	3.852		
B	linear_hexagon_V7_a	BMF-RG	0.25	0.132	4.819	0.967	5.7
C	linear_hexagon_V7_slocum	BMF-RG	0.2	0.103	4.62		
C	linear_hexagon_V7_slocum	BMF-RG	0.2	0.132	5.686	1.066	6.5
D	linear_hexagon_V7_slocum_mod	BMF-RG	0.25	0.103	4.976		
D	linear_hexagon_V7_Slocum_mod	BMF-RG	0.25	0.132	6.023	1.047	4.8
E	linear_hexagon_V8_Slocum	BMF-RG	0.25	0.103	4.606		
E	linear_hexagon_V8_Slocum	BMF-RG	0.25	0.132	5.689	1.083	8.077
Of the four options that were close or met the 1mm deflection change threshold option D had the lowest maximum stress. The table below is an inquiry into other material thicknesses for this option (option D).							
D	linear_hexagon_V7_Slocum_mod	BMF-RG	0.2	0.103	7.770		
D	linear_hexagon_V7_Slocum_mod	BMF-RG	0.2	0.132	9.084	1.314	6.47
D	linear_hexagon_V7_Slocum_mod	BMF-RG	0.15	0.103	8.222		
D	linear_hexagon_V7_Slocum_mod	BMF-RG	0.15	0.132	11.68	3.46	7.24

The above table summarizes the simulation results for a range of designs (which can be found in the table below) with the BMF resin RG.

Table 12: 3D Printed Diaphragm Geometries.

ID - File Name	Geometry
A - linear_hexagon_V7_a	
B - linear_hexagon_V7_a	
C - V7_Slocum	
D - V7_Slocum_modified	
E - V8_Slocum	

The above table summarizes the diaphragm geometries explored through simulations with BMF's 3D printed RG material.

With some very slight geometry modifications to ID E in the table above the final prototype file was created and evaluated with the table below.



Figure 38: The Final Prototype 3D Printed Diaphragm Design.

The image above is of the hexagonal diaphragm part that was 3D printed by BMF.

Table 13: 3D Printed Diaphragm Design Simulation Results - Material Thickness.

iD	File Name	Material	Thickness [mm]	Force Applied [N]	Max Deflection [mm]	Def Change [mm]	Max Stress [Mpa]	Def/max stress
D	linear_hexagon_V9	BMF-RG	0.25	0.103	4.976	---	3.9	1.28
D	linear_hexagon_V9	BMF-RG	0.25	0.132	6.023	1.047	4.9	1.23
D	linear_hexagon_V9	BMF-RG	0.2	0.103	7.770	---	5.4	1.44
D	linear_hexagon_V9	BMF-RG	0.2	0.132	9.084	1.314	6.5	1.40

The above table summarized the simulation results for the prototyped 3D printed Diaphragm design.

The designs described above were prototyped and experiments were conducted with these 3D printed Diaphragms. The details of these prototypes and experimental results can be found in the next section.

One additional idea that was experimented with but not prototyped was the option of having pre-curved beams as part of the Diaphragm. This would allow for the lower bound of the Diaphragm to be unchanged between the initial and final conditions because the deflecting beams would not be lower than the outer frame at any point during loading.

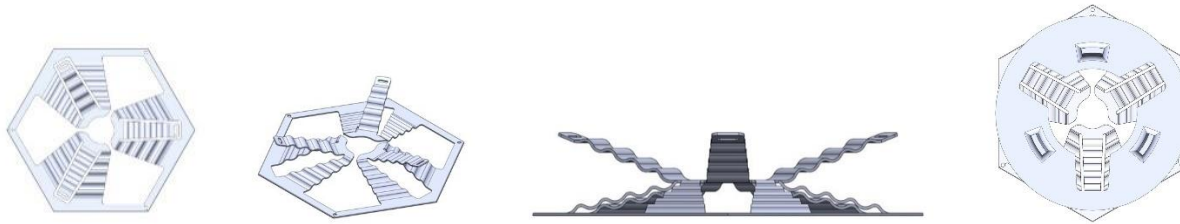


Figure 39: Pre-Curved Diaphragm Design.

The above images show a few views of the pre-curved Diaphragm design. The right most image is the only one with the vial holder included.

The prototyped set of these Diaphragms has the vial holder interfacing with the Diaphragm through tabs and slots, but subsequent designs had a more refined kinematic coupling design. The geometry of the connection between the diaphragm and vial holder was designed to be a section of two overlapping spheres so there are two points of contact in a v-groove in the Diaphragm. The v-groove in the Diaphragm was designed to be shallow to allow for ease of injection molding this component.

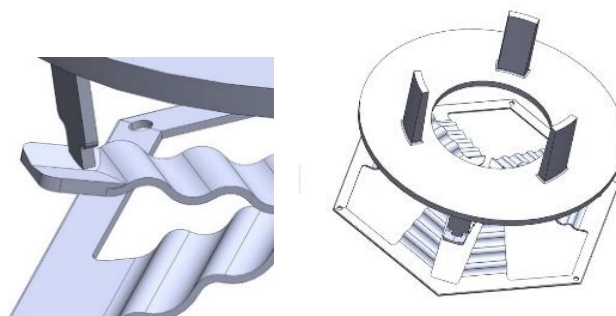


Figure 40: Pre-Curved Diaphragm Connection to Vial Holder.

The above images show details of the interface between the pre-curved Diaphragm and the vial holder.

2.1.6 Prototyping and Evaluation

The slot and tab Diaphragm design described above was 3D printed by BMF (Boston Micro Fabrication) in their RG resin. The RG resin was selected because it has material properties close to those of injection moldable plastics, is biocompatible, and does not uptake water (bmf3d, 2021).

The vial holder was printed using a Clear V4 resin on a Form 2. The images below show the prototyped parts. Some of the Diaphragms broke during shipping due to thin wall thicknesses.



Figure 41: BMF Prototypes.

The images above show the BMF 3D printed Diaphragms both before assembly into the subassembly with the vial and vial holder and after assembly.

As can be seen in the image below, the material thickness of the Diaphragm is not uniform over the full Diaphragm cross section. This was a result of the 3D printing process.

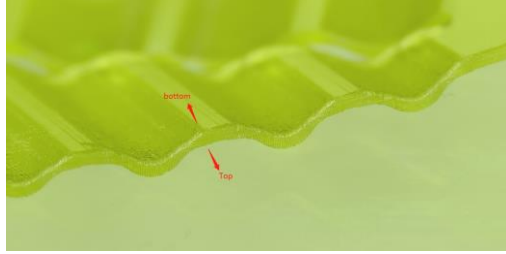


Figure 42: Image of Cross-Section of BMF Diaphragm.

The above image shows the nonuniform material thickness across the 3D printed diaphragm.

In the experiments conducted the overall deflection change was approximately 0.7mm which differed from the simulated deflection change of 1mm. Another key observation is the behavior of the Diaphragm when the weight was constant. Instead of maintaining a constant deflection for a constant weight the deflection increased with time. This set of experiments was conducted by adding 0.5mL of water in droplet increments, waiting about 10 second, and then adding the next 0.5mL of water in droplet increments. This change in deflection with a constant weight was very problematic as this introduced a time dependency on the behavior of the Diaphragm. This behavior was attributed to creep in the 3D printed material. This behavior eliminated this prototyping method as an option for Diaphragm designs.

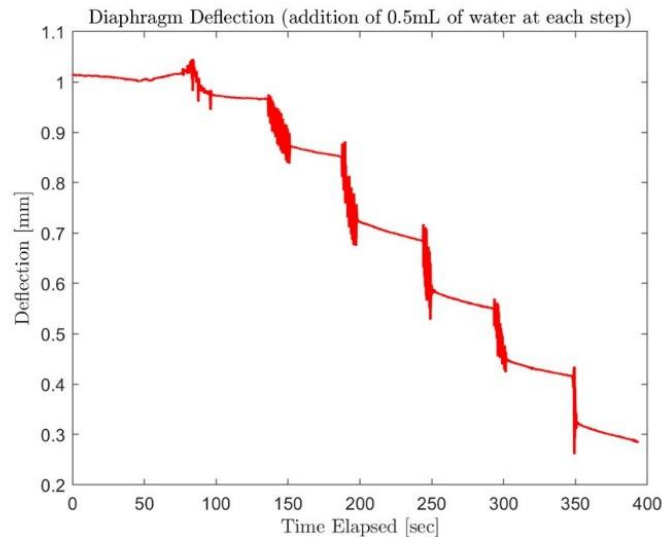


Figure 43: 3D Printed Diaphragm Experimental Results.

The above graph shows the change in deflection reading when the weight is constant at the step increments during this experiment. This change over time prevented this material and Diaphragm design from being viable for the subsystem.

Also of note, there was substantial uneven loading with this design as the center of mass was well above the Diaphragm. This uneven loading and the creep in the 3D printed material is what eliminated this material and Diaphragm design as an option for this system.

3. Sensing

The weight-sensing subsystem was designed so that weight changes could be measured through associated deflections. In order to measure these deflections two primary approaches were explored. The first approach used for the experiments described above used a laser displacement sensor. The second approach was to use imaging to read deflections. The laser displacement sensor approach is substantially more costly and has a smaller area of analysis than the imaging approach. The laser displacement sensor has a sensing spot while the imaging approach has a camera which can view a wider area. The laser displacement sensor was used in all of the experiments and the imaging approach has not been fully designed and validated at this time.

3.1.1 Laser Displacement Sensor

The Keyence CI-L070 Confocal Displacement Sensor was selected for use in this subsystem. The minimum resolution for this sensor is 0.25 microns, the reference distance is 70 mm, the measurement range is +/- 10 mm, with a spot diameter of 600 microns. These specifications met those required by the geometry of the larger system. An additional consideration for the experimental setup was that the Keyence laser displacement sensor was able to see through a ZnSe window with an antireflective coating which was the viewport material in the experimental chamber.

In the experiments described previously the laser displacement sensor used a reference surface (on one of the prongs of the vial holder) to read displacements. As each vial holder had three prongs there were three reference surfaces per vial and the deflection reading could be an

average of the three readings in the full lyophilization system. This setup also allows for the possibility of having standard reference points which are stationary and could be used as a known deflection.

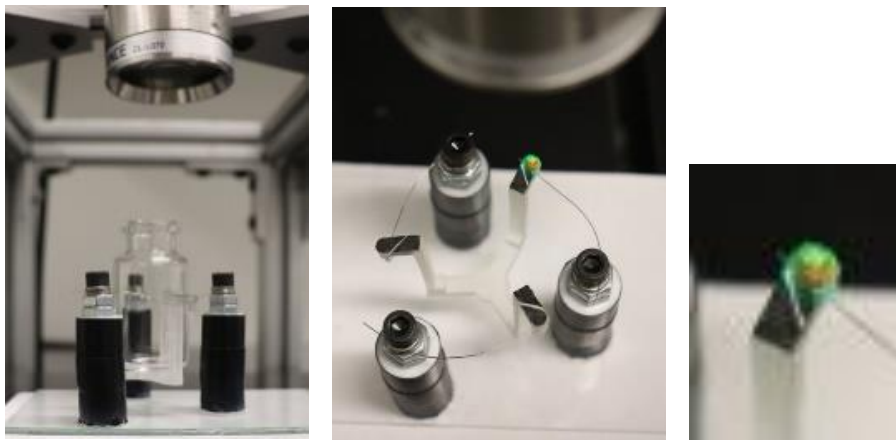


Figure 44: Keyence Laser Displacement Sensor Spot.

The images above show an experimental setup with the Keyence Laser Displacement Sensor and also show a close up of the colorful sensing spot on one of the prongs of the vial holder.

To read an entire array of vials an array of Keyence laser displacement sensors would be used. This approach would be fairly costly which is what led to the exploration of imaging displacement as an alternative way to read displacements.

3.1.2 Imaging Displacement

The Keyence Laser Displacement Sensors are fairly expensive especially when an array of sensors is needed to measure multiple small-area locations at once. The imaging approach reduces the cost and increases the area over which displacements can be read. In its simplest form the imaging approach is to take pictures of the weight-sensing subsystem and to compare the migration of key locations over time and then determine the deflection and therefore the current weight of the product. If the key locations that are tracked are crossing points between a straight or curved spring and a grid as the spring moves above the fixed grid then the moiré effect allows for the measurement of very small displacements of the spring.

The Bent Spring design, the final design which yielded sufficient deflection and was stable, did not have enough spring displacement in the x-y plane (parallel to the base surface) to measure the displacement with unprocessed images taken from above looking at the motion of the springs. This does not mean that imaging displacement is not feasible for the Bent Spring design. There are other methods which introduce projected grids through gratings which enable z-direction deflection to be read by a camera above the vials. Additionally, there may be options to process the images or take higher quality images which could help resolve the small displacements. This is an area which requires future work before becoming viable.



Figure 45: Displacement of Springs From Above.

The image above shows an experimental setup for attempting to measure the displacement of the springs in relation to the grid below. The experimental results indicated that the wire displacements could not be measured with unprocessed images.

The imaging approach also was able to be applied to the Partial Loop spring design, the Diaphragm design, and the Triangle Flexure design. The displacements in the x-y plane were not large enough to use unprocessed images and no projected gratings for any of these options. In the Partial Loop spring design, the option with the most x-y plane displacement, the spring profile displaced in relation to a grid below. The option to analyze area changes of the trapezoids formed by the grating and the wire was also explored. With the Diaphragm design teeth could be introduced along the deflecting beams and the changes in relative areas could be read. In the flexure design the stationary triangles could have gratings which would be compared to the corresponding gratings on the deflecting petals.

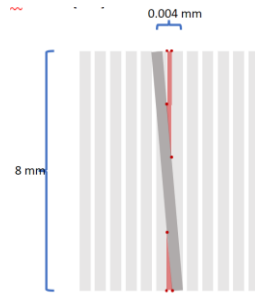


Figure 46: Example of Measuring Relative Areas for Wire Displacement.

The above figure shows an example of the area measurements that could be read around a moving wire. The changes for areas could be related to spring displacement and then the deflection.

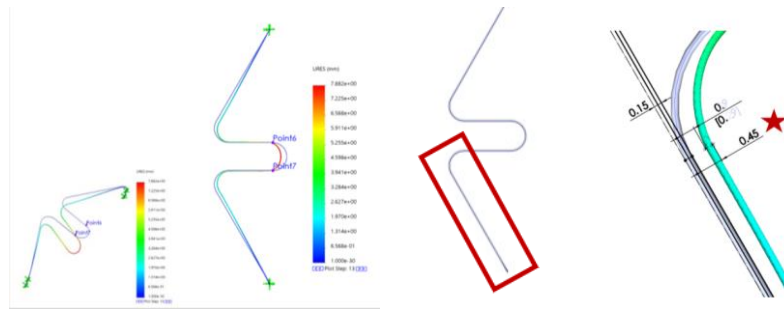


Figure 47: Example of Partial Loop Displacement.

The above figure shows an example of how the Partial Loop wire path is simulated to shift with the weight changes.

The Keyence laser displacement sensor has worked well experimentally and will continue to be a good sensing option. The imaging approach would reduce the cost substantially and would be a nice sensing approach to utilize but is not necessary for the functionality of the weight-sensing subsystem.

4. Conclusion

The Bent Spring design and the Keyence laser displacements sensor make up a weight-sensing subsystem which has the ability to measure the change in weight of product that is proceeding through a larger lyophilization system with the ability to measure down to a 0.1% water content in the dried product. This allows for monitoring of product weight which in turn allows for monitoring of product conditions through the array of vials. The ability to individually monitor the product weight in each vial allows for active control of the system parameters to ensure the product is uniform within an array and has sufficiently low water content at the completion of the lyophilization process.

5. Future Steps

The next steps with the Bent Spring design would be to run additional experiments to help characterize the behavior of the spring assemblies in the lyophilization conditions and to work on the design for manufacturing of the Bent Spring design.

Additional work can be done with the imaging displacement approach to validate that approach. As the subsystem is integrated into the larger system the cost and complexity of the Keyence laser displacement sensor will continue to make the imaging displacement approach appealing.

6. Bibliography

- bmf3d*. (2021). Retrieved from BMF Boston Micro Fabrication: <https://bmf3d.com>
- Cedric Garion, B. S. (2006). Constitutive modelling and identification of parameters of the plastic strain-induced martensitic transformation in 316L stainless steel at cryogenic temperatures. *International Journal of Plasticity*.
- Giovanni, M. D. (1982). *Flat and Corrugated Diaphragm Design Handbook*. Boca Raton: CRC Press .
- Jocelyn Kluger, A. S. (2017). Ring-Based Stiffing Flexure Applied as a Load Cell with High Resolution and Large Force Range. *Journal of Mechanical Design*.
- Laurens De Meyer, J. L. (2019). Dual chamber cartridges in a continuous pharmaceutical freeze-drying concept: Determination of the optimal dynamic infrared heater temperature during primary drying. *International Journal of Pharmaceutics*.
- Luigi C. Capozzi, B. L. (2019). From Batch to Continuous : Freeze-Drying of Suspended Vials for Pharmeseuticals in Unit-Doses. *Industrial & Engineering Chemistry Research*.
- Roberto Pisano, A. A. (n.d.). Achieving Continuous Manufacturing in Lyophilization: Technologies and Approaches.
- Slocum, A. (1999). *United States of America Patent No. 5973394*.

